



AATSR
Test Report

Doc No: PO-TR-RAL-AT-0023

Issue: 2

Date: 08 July 1999

AATSR Visible Calibration Report

Prepared by:

D.L. Smith

Date

Checked by:

J. Delderfield

Date

Approved by:

T. Edwards

Date

Document Change Record

Issue	Date	Affected Pages	Comments
1	23-Mar-99	All	First Issue
2	8-Jul-99	6,8,10,13,14,22,32,34-37,50-53	Calibration figures for integrating sphere take account of post calibration data.

Contents

1 Acronyms.....4

2 Applicable Documents.....5

3 Scope of Document.....6

4 Test Requirements6

5 Calibration Algorithms7

 5.1 General7

 5.2 Integrating Sphere Calibration.....8

6 Calibration of Sources10

 6.1 Large Integrating Sphere10

 6.2 Polarisation Filters.....15

7 Instrument Calibration17

 7.1 Experiment17

 7.2 Radiometric Response21

 7.3 Radiometric Noise22

 7.4 VISCAL.....25

 7.4.1 Reflectance Factor25

 7.4.2 Used Pixels and Uniformity.....25

 7.5 Polarisation.....28

 7.6 Scan dependent effects30

 7.7 Uniformity of response across aperture.....31

8 Summary and Conclusions33

Appendix A Test Plan Summary35

Appendix B 1.6µm Calibration36

Appendix C Visible Channel Spectral Response.....40

Appendix D Source Calibration – Raw Data.....48

Appendix E Calibrated AATSR Input Radiances.....52

Appendix F Test Data Files56

Appendix G NPL Calibration Certificate **Error! Bookmark not defined.**

1 Acronyms

ATSR	Along Track Scanning Radiometer
AATSR	Advanced Along Track Scanning Radiometer
ACTS	AATSR Calibration and Test System
CRC	Cyclic Redundancy Check
DEU	Digital Electronics Unit
EGSE	Electrical Ground Support Equipment
FPA	Focal Plane Assembly
IEU	Instrument Electronics Unit
IFOV	Instantaneous Field of View
IR-FPA	Infra Red Focal Plane Assembly
IVR	Infrared and Visible Radiometer
MDA	Measurement Data Adapter
NIST	National Institute for Standards and Technology (USA)
NPL	National Physical Laboratory (UK)
RAL	Rutherford Appleton Laboratory
RMS	Root Mean Squared
TCADS	Tank Control and Data System
UDT	United Detector Technology
VISCAL	Visible Calibration System

2 Applicable Documents

AD 1	PO-RS-GAD-AT-0002	AATSR Instrument Performance Requirements - Issue 2
AD 2	PO-PL-RAL-AT-0014	AATSR Test and Calibration Plan - Issue 2
AD 3	PO-PR-RAL-AT-0026	AATSR Visible Calibration Procedures - Issue 1
AD 4	PO-SW-BAE-AT-0002	Statement of Work for AATSR VISCAL and Cooler Subsystem, Instrument Calibration, Australian Shadowing and System Consultancy - Issue 1
AD 5	ER-TN-RAL-AT-2173	ATSR-2 Commissioning Report - Issue 1
AD 6	PO-TN-RAL-AT-0165	AATSR VISCAL Calibration Parameters
AD 7	PO-TN-AUS-AT-1014	AATSR FM02 Spectral Response
AD 8	QD21/98/011/ADE1 (NPL ref.)	NPL Certificate of Calibration for Spectral Radiance of the U2000 Integrating Sphere

3 Scope of Document

This document describes the AATSR visible calibration tests defined in the calibration plan, AD 2 as required by AD 1. This fulfils the tasks defined in section 8.1.2 of RAL's statement of work, AD 4.

Since the first issue of this document the full aperture radiances of main calibration source had been remeasured by NPL, AD 8. Although there was good agreement between the RAL and NPL measurements at the short wavelengths, there was a significant difference at 1.6 μ m.. This could be explained by difficulties in accurately measuring radiances at 1.6 μ m using the RAL method. Because of the higher level of traceability to primary standards, the NPL calibration is used for the absolute radiometric calibration, and the RAL measurements for the variation in signal with aperture size. The revised calibration affects only the absolute radiometric response of the visible channels, whereas the results of the VISCAL calibration, measurements of scan dependent effects, and polarisation sensitivity measurements are unaffected.

4 Test Requirements

The requirements for the pre-launch calibration of the AATSR Visible channels defined in AD 2 are:

- Measure the detector response as a function of source input intensity over the expected operational range to an absolute accuracy < 5%.
- Determine the calibration level of the VISCAL unit.
- Measure the Radiometric Noise.
- Determine and measure any scan dependent effects by measuring the response at all points around then Nadir and Along-Track views.
- Characterise the variation of the normalised radiometric response due to polarisation to better than 0.5%.

The initial scope of the calibration applied only to the 0.87 μ m, 0.66 μ m and 0.56 μ m channels. This has since been extended to include the 1.6 μ m channel to meet requests from the AATSR user community. Originally, the 1.6 μ m channel was to be solely used for cloud detection in the sea-surface-temperature retrieval, and hence did not need to be calibrated. However, the 1.6 μ m channel on ATSR-2 has proved vital for cloud properties and fire scar quantification. The cloud measurements alone make it necessary for the 1.6 μ m channel to be calibrated to a similar accuracy as the other visible channels.

5 Calibration Algorithms

5.1 General

The AATSR visible/near-infra-red channels, at 1.6 μm , 0.87 μm , 0.66 μm and 0.56 μm are designed to measure reflected solar radiation. The reflectance of a scene, r_{scene} at wavelength λ may be determined from the radiance measured by AATSR, L_{scene} , the spectral bandwidth of the channel $d\lambda$, and known values of the solar spectral irradiance, $I_{0,\lambda}$ using

$$\boxed{r_{\text{scene}} = \frac{\pi L_{\text{scene}}}{I_{0,\lambda} d\lambda}} \quad \text{eq. 5.1}$$

The scene radiance is derived from the detector counts using

$$L_{\text{scene}} = \alpha (C_{\text{scene}} - C_{\text{dark}}) / \text{Gain} \quad \text{Wcm}^{-2}\text{sr}^{-1} \quad \text{eq. 5.2}$$

where α is the calibration coefficient, *Gain* is the commanded gain of the channel and C_{dark} is the zero radiance counts which is taken as the signal from the cold on-board black-body. This is similar to the standard method used for AVHRR, SPOT and other instruments without an in-flight calibration system.

The VISCAL system on AATSR gives a signal, L_{scene} corresponding to a reflectance r_{viscal} . Substituting this into equations 5.1 and 5.2 give

$$\boxed{r_{\text{scene}} = r_{\text{viscal}} \frac{C_{\text{scene}} - C_{\text{dark}}}{C_{\text{VISCAL}} - C_{\text{dark}}}} \quad \text{eq 5.3}$$

Here there is no need to know the solar irradiance or spectral bandwidth. The viscal reflectance factor may be derived using the optical properties and geometry of the components such that

$$\boxed{r_{\text{viscal}} = \frac{A_{M2}}{A_{\text{AATSR}}} \cos\left(\frac{\pi}{4}\right) r_{M1} r_{M2} \tau_{UV} R_{\lambda}\left(0, \frac{\pi}{4}\right)} \quad \text{eq. 5.4}$$

where

A_{M2} is the footprint area of mirror M2 on the opal = 34.08cm²†

A_{AATSR} is the area of the instrument aperture = 95cm²

r_{M1} and r_{M2} are the reflectances of mirrors M1 and M2

τ_{UV} is the transmission of the uv filter

† The VISCAL ADP stated this to be 32.4cm² but this has been revised as a result of the instrument level tests.

and $R_\lambda(0, \frac{\pi}{4})$ is the bidirectional reflectance of the opal illuminated at normal incidence and measured at 45° to normal.

These parameters and the calculated reflectance factors are given in Table 5-1.

Parameter	0.56μm	0.66μm	0.87μm	1.6μm
FM Opal 0/45° Radiance Factor (%)	96.0 ± 0.8	96.1 ± 0.8	95.0 ± 2.0	90.0 ± 2.2 ¹
FM UV Window Transmittance (%)	92.2 ± 1.0	92.5 ± 1.0	92.7 ± 1.0	92.7 ± 1.0
FM Mirror M1 Reflectance (%)	84.9 ± 1.0	84.2 ± 1.0	82.9 ± 1.0	95.0 ± 1.0
FM Mirror M2 Reflectance (%)	86.4 ± 1.0	85.7 ± 1.0	84.0 ± 1.0	95.7 ± 1.0
VISCAL Reflectance Factor	0.165 ± 0.003	0.163 ± 0.003	0.156 ± 0.004	0.192 ± 0.005

Table 5-1: AATSR VISCAL optical properties and derived reflectance factors The opal radiance factors were measured by NPL, and the mirror reflectances and UV window transmission were measured by Bentham Instruments (see AD 6 for references).

The main objectives of the pre-launch calibration is to determine by experiment the responsivity factors, α_λ and VISCAL reflectance factors, $r_{\lambda, \text{VISCAL}}$ for each channel

5.2 Integrating Sphere Calibration

As described in §6.1 the full aperture radiance of the integrating sphere was calibrated by NPL, AD 8. The output as a function of aperture area was measured at RAL using a radiometer with an active area, A_{Rad} cm², at a distance $D_{\text{Sphere-Rad}}$ cm from the sphere aperture. The radiance from the integrating sphere, L_{sphere} can be derived from the flux measured by the radiometer, using

$$L_{\text{sphere}} = \Phi_{\text{rad}} \frac{D_{\text{sphere-rad}}^2}{A_{\text{rad}} A_{\text{aperture}}} \quad \text{Wcm}^{-2} \text{sr}^{-1} \quad \text{eq. 5.5}$$

Because the beam of AATSR is collimated and the sphere is ~1m from the aperture it can be assumed that $A_{\text{aperture}} = A_{\text{AATSR}} = 95\text{cm}^2$, hence for direct illumination of the AATSR foreoptics

$$L_{\text{direct}} = \Phi_{\text{rad}} \frac{D_{\text{sphere-rad}}^2}{A_{\text{rad}} A_{\text{AATSR}}} \quad \text{Wcm}^{-2} \text{sr}^{-1} \quad \text{eq. 5.6}$$

¹ As the opal 0°/45° reflectance factor at 1.6μm has not been measured for AATSR the value given for ATSR-2 has been used. Since the spectral characteristics at the shorter wavelengths between the AATSR and ATSR-2 opals are within 1% of each other we can be confident that the 1.6μm radiance factor is also within this margin. The error quoted includes this additional uncertainty.

The signal channel responsivity is determined by plotting the measured signal (as volts into the analogue to digital converter) for a range of input radiances, L_{direct} . The input voltage at the ADC is related to the digital pixel counts, their nominal relationship being:

$$V_{in} = \frac{8.6}{2^{14}}(Offset - 2^{13}) - \frac{C}{5 \times Gain} \quad \text{eq. 5.7}$$

When the integrating sphere is positioned to illuminate the VISICAL, the total illumination at the opal generated by the integrating sphere is

$$\begin{aligned} \Phi_{opal} &= L_{sphere} \frac{A_{opal} A_{source}}{D_{source-opal}^2} \\ &= \Phi_{rad} \frac{D_{sphere-rad}^2}{D_{sphere-opal}^2} \frac{A_{opal}}{A_{rad}} \quad \text{W} \end{aligned} \quad \text{eq. 5.8}$$

The irradiance at the opal is then

$$\begin{aligned} I_{opal} &= \frac{\Phi_{opal}}{A_{opal}} \\ &= \Phi_{rad} \frac{D_{sphere-rad}^2}{D_{sphere-opal}^2} \frac{1}{A_{rad}} \quad \text{Wcm}^{-2} \end{aligned} \quad \text{eq. 5.9}$$

AATSR will measure radiance $L_{VISICAL}$ and substituting I_{opal} for $I_{od\lambda}$ in equation 5.1 yields

$$\boxed{r_{VISICAL} = \frac{\pi L_{VISICAL}}{I_{Opal}}} \quad \text{eq. 5.10}$$

The factor $r_{Visical}$ is the slope of a straight fit to $L_{visical}$ versus the known input radiance I_{opal}/π .

6 Calibration of Sources

6.1 Large Integrating Sphere

The primary source used for calibrating the AATSR visible channels was a Labsphere Unisource 2000, 500mm diameter, integrating sphere with a 200 mm exit aperture. The unit provided eight distinct output levels of uniform illuminance over the exit port. This was achieved by four internal lamps, two 45W and two 150W, equally spaced about the exit port. All lamps had a colour temperature of 3000K (Figure 6.1) and so the spectral profile was independent of the lamp combination used. Additional output levels were obtained by varying the area of the output aperture. This was done by inserting a blackened aluminium plate with a hole of the required diameter in front of the main aperture. A total of 27 apertures were used, including the main aperture.

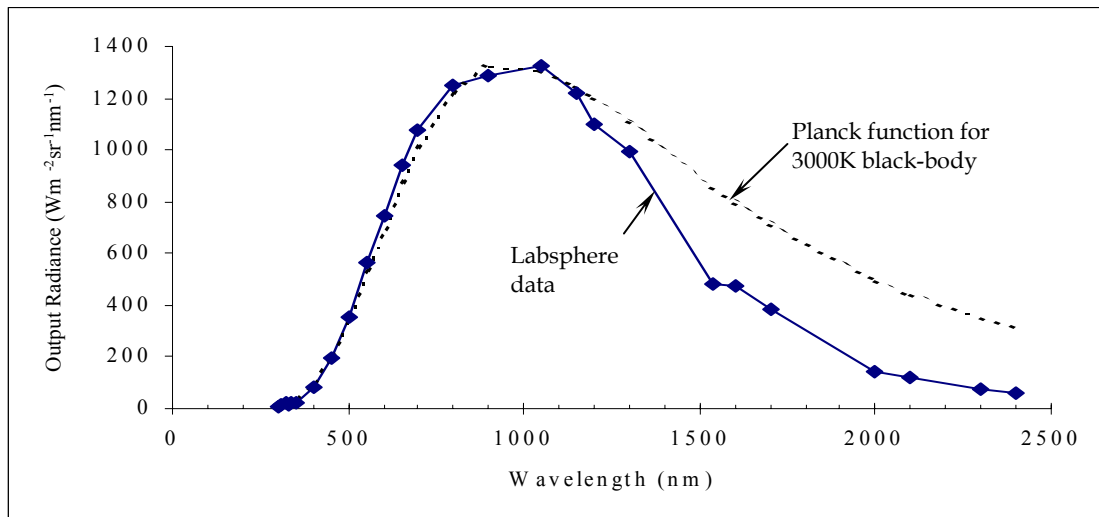


Figure 6.1: Labsphere measurement of spectral radiance of Unisource 2000 Integrating Sphere (serial no. 001205) with all lamps on.

The full aperture spectral radiances of the sphere were calibrated between 0.4 μ m to 1.6 μ m in March 1999 by NPL to recognized national standards, AD 8. In addition, before the calibration of AATSR, the output of the integrating sphere was measured by RAL at each visible channel wavelength for a range of power levels and each aperture. This was performed using a UDT 370 radiometer originally calibrated by in December 1990 against standards traceable to NIST and since recalibrated at NPL in December 1998.

The radiometer detector was positioned on the sphere axis 1096mm from the main aperture, as shown in Figure 6.2. Two detectors were used: a silicon detector with a 1cm² active area was for the 0.4-1.0 μ m range and a germanium detector with an active area of 0.2cm² covering 0.8 μ m to 1.8 μ m.

To cut out any stray light, a light tight enclosure was built, and baffles inserted between the radiometer and the integrating sphere. The internal surfaces of the box were blackened to minimize any strays from the source. This arrangement reduced the background signal to the noise levels of the radiometer.

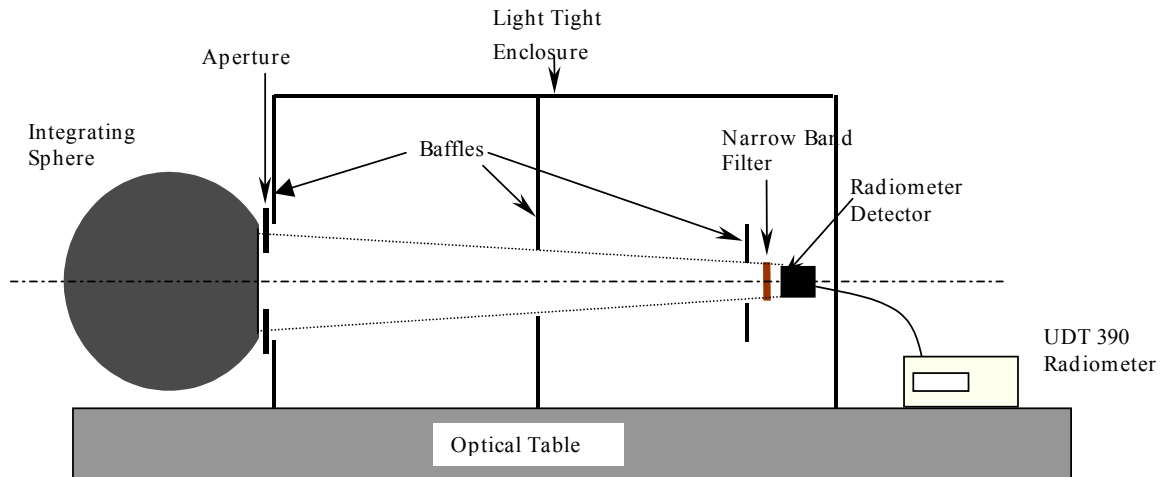


Figure 6.2: Experimental layout for calibration of the Labsphere Unisource 2000 Integrating Sphere.

Narrow band filters were inserted in front of the detector to obtain the signal at each AATSR wavelengths. The filters used were from the same batch used in the ATSR-2 and AATSR visible focal-plane-assemblies. For the 1.6 μ m channel, a commercial filter was used, as no witness filter was available. The spectral responses of these filters were measured at Bentham instruments immediately after the sphere calibration was performed. The centre wavelength, bandwidth and peak transmissions of these filters are given in Table 6-1 below. The spectral response data for the flight filters were obtained from measurements made by Auspace, AD 7 and Appendix C.

Channel	Filter Set	Mid Wavelength	Bandwidth (nm)	Transmission
0.56 μ m	AATSR Flight	0.560	20.79	0.4624
	AATSR Witness	0.560	20.09	
	ATSR-2 Witness	0.558	21.22	
0.66 μ m	AATSR Flight	0.660	20.13	0.6771
	AATSR Witness	0.659	20.69	
	ATSR-2 Witness	0.657	20.41	
0.87 μ m	AATSR Flight	0.863	20.14	0.7301
	AATSR Witness	0.863	20.25	
	ATSR-2 Witness	0.863	21.65	
1.6 μ m	AATSR Flight	1.594	62.88	0.6130
	Northern Optics	1.610	166.79	

Table 6-1: Centre wavelength, bandwidth and peak transmission of filters used for calibrating the visible calibration source.

The flux from the sphere was measured at each wavelength for all apertures at lamp powers of 45W, 90W, 150W, 240W and 390W. It is apparent from the data that the ATSR-2 visible filters were far superior to the AATSR items, see Appendix A. The output of the sphere should be a simple product of the full aperture flux, Φ_{full} , at power level P, and some function of the aperture area F(A)

$$\Phi_{n,P} = \Phi_{full,P} F(A) \quad \text{eq. 6.1}$$

This is demonstrated by normalising the measurements to the full aperture readings and plotting against aperture. The result for the 0.87 μm AATSR witness filter is given Figure 6.3. A similar result was obtained for all the other filters.

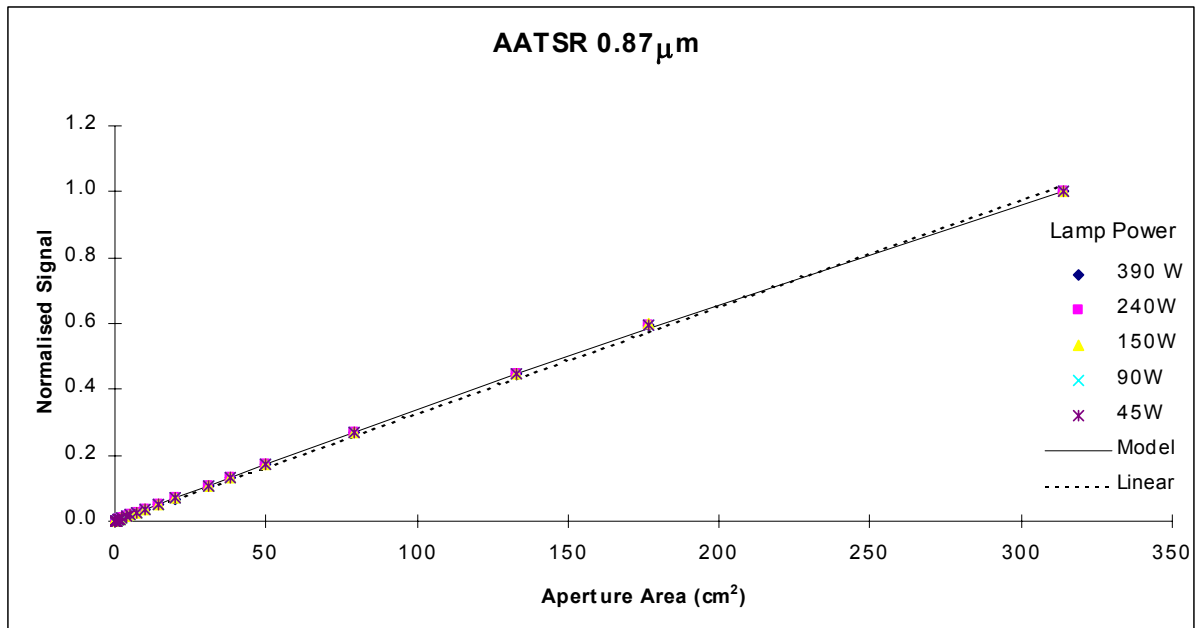


Figure 6.3: Integrating sphere flux at 0.87 μm normalised to the full aperture reading versus the exit aperture area. This plot shows that the variation in signal with aperture area is independent of the lamp intensity.

It was expected that the output signal would be directly proportional to the area of the exit aperture. However, Figure 6.3 shows that this was not the case. Initially it was assumed that this effect was due to the radiometer's view of the integrating sphere at large apertures being obstructed by the baffle arrangement. However, it has since been realized that the non-linearity relates to how the sphere acts as an enclosure.

Although the aluminium apertures were painted black, they still had a residual reflectance, r_{plate} . This means that some fraction of the sphere output that was blocked by the smaller aperture, is reflected back into the sphere, Φ_{refl} . This will be proportional to the area of the plate blocking the main 200mm aperture such that

$$\Phi_{refl} = r_{plate} \Phi_{full} (A_{full} - A_n) / A_{full} \quad \text{eq. 6.2}$$

A fraction of this will be reflected back towards the entrance aperture to give an increase in the sphere radiance. Ignoring second order effects the variation with aperture area can be approximated using

$$F(A) = (1 + R(A_{full} - A_n) / A_{full}) A_n / A_{full} \quad \text{eq. 6.3}$$

where R is effectively a product of all the internal reflectances and is obtained for each wavelength by fitting to the measured data as shown in Figure 6.3. However, this model was only really needed for the 1.6 μm channel where the radiometer readings for small apertures were within the noise limits.

To obtain the fluxes over the AATSR bandwidth we need to correct for the witness filter transmission and bandwidth using

$$\Phi_{rad} = \frac{\Phi_{meas} d\lambda_{AATSR}}{\tau_{filter} d\lambda_{Filter}} \quad \text{eq. 6.4}$$

Using the full aperture spectral radiances from the NPL calibration at the AATSR wavelengths and multiplying with the channel bandwidth, $d\lambda$, we obtain the AATSR integrated radiances in Table 6-2. The previous RAL measurements are given in brackets for comparison.

Power Level (W)	Integrating Sphere Radiance $\text{mWcm}^{-2}\text{sr}^{-1}$			
	1.6 μm	0.87 μm	0.66 μm	0.56 μm
390	7.55 (9.94)	7.41 (7.46)	5.73 (5.26)	3.43 (3.42)
240	4.51 (6.01)	4.43 (4.45)	3.41 (3.16)	2.05 (2.05)
150	3.09 (4.04)	3.04 (3.03)	2.34 (2.13)	1.40 (1.38)
90	1.51 (1.95)	1.48 (1.48)	1.14 (1.06)	0.68 (0.69)
45	0.77 (0.98)	0.75 (0.74)	0.58 (0.53)	0.35 (0.35)

Table 6-2: Full aperture radiances of integrating sphere over the AATSR visible channel bandwidths obtained from NPL calibration. The radiometric accuracy is 3.2% at 0.56 μm and 0.66 μm , 3.4% at 0.87 μm and 8.7% at 1.6 μm . The numbers in brackets are the measurements made by RAL.

The data in Table 6-2 shows very good agreement between the RAL and NPL calibrations at 0.87 μm and 0.56 μm . At 0.66 μm , the RAL readings are consistently 6.5% lower than the NPL values, traced to a slight misalignment of the witness filter in the RAL setup. Better agreement (<2% difference) was achieved when the measurements were repeated at RAL, taking extra care to ensure that the filters were optimally aligned. At 1.6 μm there is a significant difference

between the RAL and NPL measurements. The differences and the lower accuracy of the NPL calibration highlight the difficulty in measuring radiances in the near infrared. The differences are attributable to a combination of effects; error in the filter transmission, area of the detector aperture and, more significantly, radiometric leaks and strays.

The radiance measured by AATSR for a given aperture and power setting is then

$$L_{n,P} = L_{full,P} F(A_n) . \quad \text{eq. 6.5}$$

Except where the sphere aperture is larger than the AATSR aperture (=95cm²), then

$$L_{n,P} = L_{full,P} F(A_n) A_{AATSR} / A_n . \quad \text{eq. 6.6}$$

The resulting look up tables used for calibrating the AATSR visible channel radiometric responses are given in Appendix C.

The main sources of uncertainty in the sphere calibration are

- Full aperture radiance calibration - from NPL data, AD 8
- Distance from radiometer to sphere = 5mm (= 5/1096 = 0.5%)
- Sphere Drift - estimated from repeat measurements of the integrating sphere over time.

The values assigned to each of these, and the total RMS error are given in Table 6-3 below.

Source	1.6μm	0.87μm	0.66μm	0.56μm
Radiometer Calibration	8.7%	3.4%	3.2%	3.2%
Sphere Drift	0.5%	0.5%	0.5%	0.5%
Geometric Errors	0.5%	0.5%	0.5%	0.5%
Total RMS Error	8.7%	3.5%	3.3%	3.3%

Table 6-3: Summary of errors in calibration of integrating sphere.

6.2 Polarisation Filters

For the polarisation sensitivity measurements a smaller 30W integrating sphere was used. Two standard Ealing polarisation filters were used, one for the visible range from $0.2\mu\text{m}$ to $0.8\mu\text{m}$, and the other to cover the infrared range from $0.8\mu\text{m}$ to $2.2\mu\text{m}$. The polarisers were mounted in rotatable mounts so that their variation in response could be measured as a function of polarisation angle. A calcite polariser was used to determine the orientation of the filters in the Figure 6.4 test set-up.

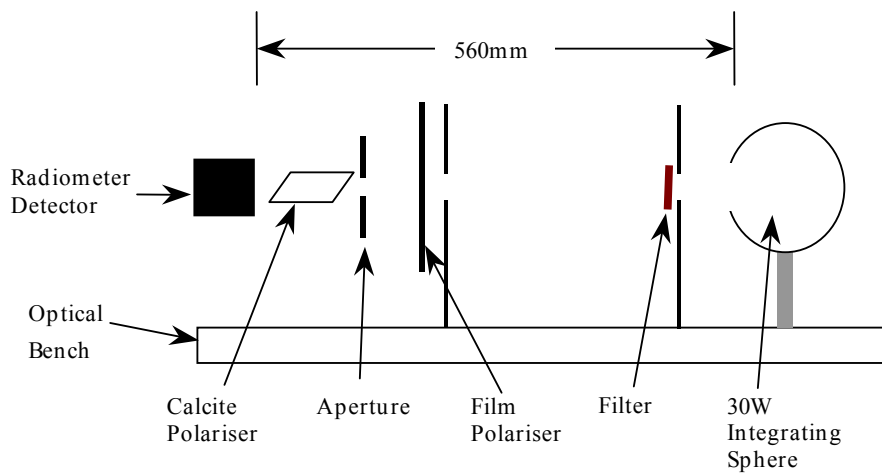


Figure 6.4: Test arrangement for calibrating the orientation of the thin film polarising filters.

Before establishing the relative orientation of the polarisers, it was essential to measure any polarisation from the integrating sphere. Radiometer readings were taken for all filter and detector combinations. The variation in measured signal, relative to the mean sphere output, was less than $\pm 0.5\%$ for all wavelengths, Figure 6.5.

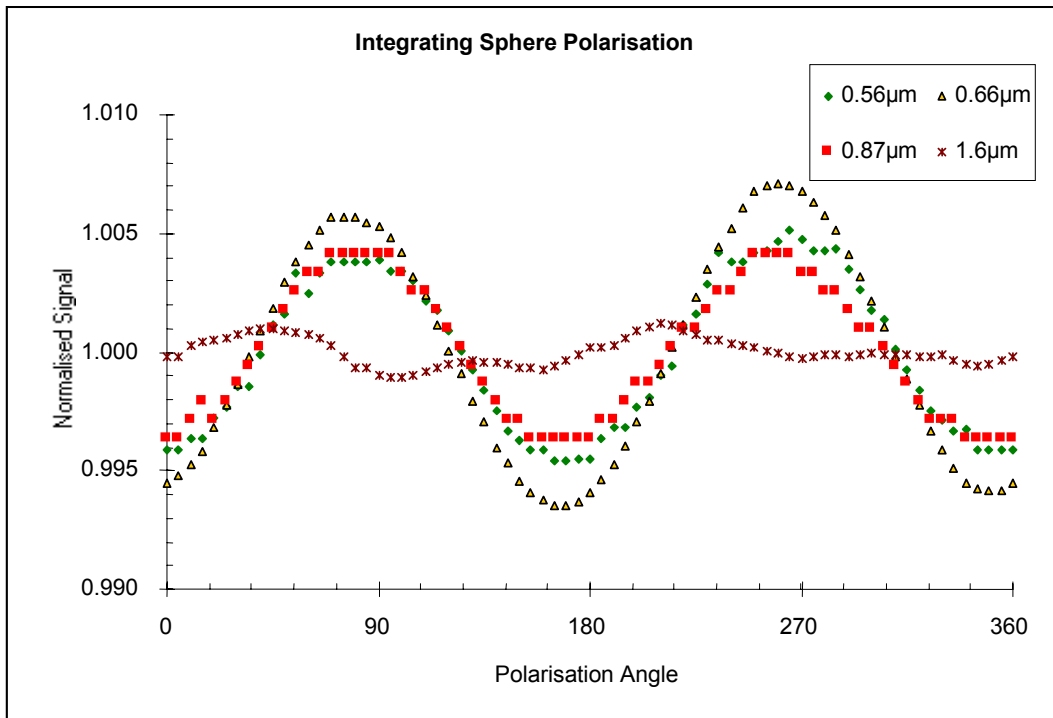


Figure 6.5: Measured variation of 30W integrating sphere output with polarisation angle. The polarisation sensitivity of the radiometer was removed by performing the measurements with the detector set at orthogonal orientations. The variation at 1.6µm is mainly due to signal drift.

The calcite polariser was inserted into the light path and oriented so that the plane of the polarised light was perpendicular to the optical bench. Radiometer readings were again taken for each detector and filter combination. The results showed that the visible filter was well set up in the rotating mount and required no correction. The data for the IR filter showed that it was offset by -60° in the mount and therefore a corresponding correction was required.

7 Instrument Calibration

7.1 Experiment

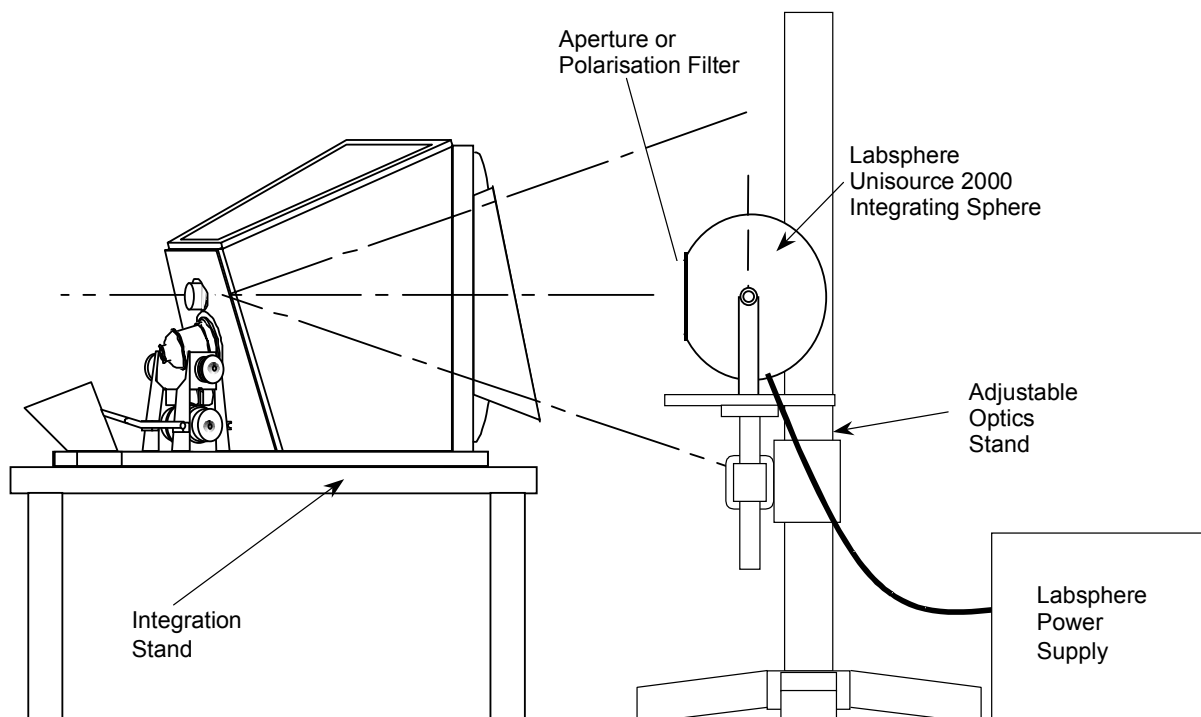


Figure 7.1: Test configuration for AATSR visible channel calibration. For the VISCAL measurements, the source was positioned at the entrance of the VISCAL unit. For the polarisation sensitivity measurements, the U2000 source was replaced with the 30W integrating sphere and polarisation filters.

The AATSR instrument was mounted on the integration stand, as shown in Figure 7.1, and was powered into MEASUREMENT mode with the scan mirror stationary.

For the radiometric response and polarisation measurements, the sphere was positioned a short distance from the centre of the nadir aperture. Precise alignment of the sphere with the instrument was performed as follows. First, the sphere was illuminated with the 45W lamp on and the 100mm aperture installed. Using the default detector gains and offsets, the scan mirror was rotated by hand until the maximum signal was obtained. After this, the sphere was scanned across the beam in horizontal and vertical axes, and the detector response was measured at 5mm intervals. The sphere was finally located at the position where the maximum signal was obtained. Because of the small divergence of the instrument's optical beam

(~1.3mm / m), the distance between the sphere and the scan mirror was not critical for these measurements. However this distance was recorded and maintained for all measurements.

The alignment procedure for the VISICAL throughput measurements was similar. Here, the sphere was positioned at the entrance baffle of the VISICAL unit, and aligned so that the axis of the sphere was in line with the centre of the baffle. The plane of the entrance aperture was set parallel to the opal surface. The distance from the sphere aperture to the entrance baffle was measured to be $110\pm 5\text{mm}$, giving a total distance from the sphere to the opal of $480\pm 5\text{mm}$. In this case, the distance between the sphere and opal was critical, so great care was taken to ensure that the sphere was set to exactly the same position for each set of measurements. Once the sphere was aligned, all lamps were switched on and detector gains were set to full scale to obtain the maximum possible response. The scan mirror was then rotated by hand until the highest signal was reached. This was a delicate process and required great patience to achieve the optimum position.

The visible calibration tests were performed in three stages

1. The FPA in air
2. The FPA in vacuo at room temperature
3. The FPA in vacuo and the IR FPA cooled to 80K.

To allow a response in the visible channels whilst the FPA was under vacuum, the vacuum flange mounted over the FPA baffle tube, was fitted with a ZnSe window. The transmission of the window was measured for the $0.87\mu\text{m}$, $0.66\mu\text{m}$ and $0.56\mu\text{m}$ channels by comparing the in air responses with the cover in place and removed, Table 7-1. At $1.6\mu\text{m}$, the manufacturer's measurement was used since it was not possible to perform the test at this wavelength.

Channel	Transmission
$1.6\mu\text{m}$	0.945
$0.87\mu\text{m}$	0.922
$0.66\mu\text{m}$	0.886
$0.56\mu\text{m}$	0.805

Table 7-1: Transmission of ZnSe window over FPA baffle tube.

Science data packets from the DEU were acquired by the measurement data adapter (MDA) of the EGSE. These were combined with the contemporaneous data from the AATSR Test and Calibration System (ACTS) which recorded the temperature of the integrating sphere. For a calibration measurement, the routine GET_VIS was used to capture a number of packets (usually 10) from the measurement data stream, and process these to obtain the following parameters:

- Average pixel counts (1.6, 0.87, 0.66 and $0.56\mu\text{m}$)
- Standard deviation of pixel counts (1.6, 0.87, 0.66 and $0.56\mu\text{m}$)
- Integrating sphere power level
- Integrating sphere aperture setting
- Distance of source from instrument
- Polarisation angle

Detector gains and offsets (1.6, 0.87, 0.66 and 0.56 μ m)
Integrating sphere temperature
Instrument time stamp
IEGSE time stamp
ACTS time stamp.

The above parameters were written to a text file, which was appended each time the routine was run. (The file name included the test number and the date of the test). A new output file was created for each day and new test. The raw data was also stored to a separate binary file for reprocessing if necessary. It should be noted that before processing the data, GET_VIS inspected the data packets for CRC errors, missing or duplicate packets, packet write errors and instrument housekeeping telemetry out of limits. If any such errors occurred during a measurement, the data were not recorded.

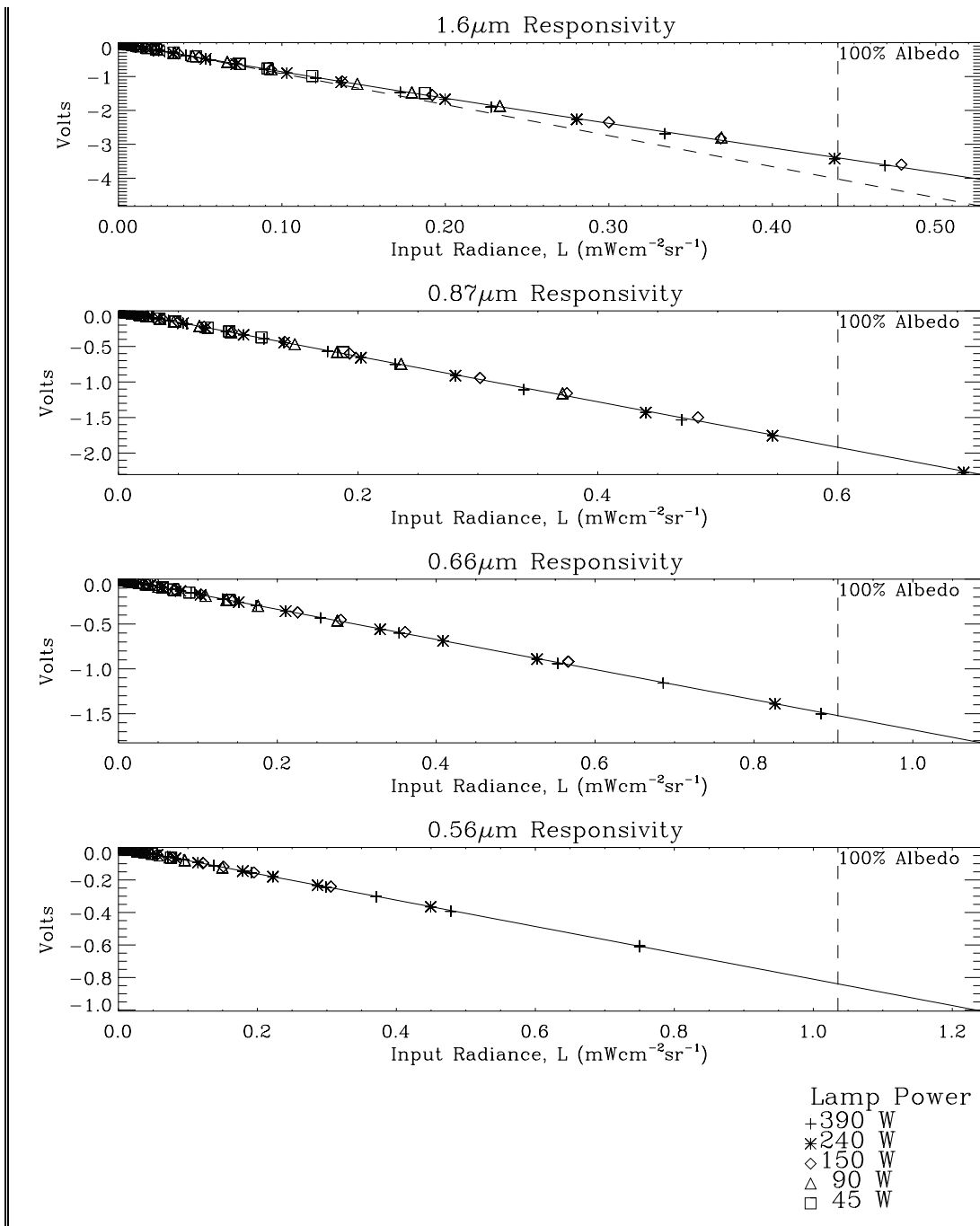


Figure 7.2: AATSR visible channel response (ADC input voltage) vs. sphere radiance for the test case with the IR-FPA cooled to 80K. The lamp settings used for the measurements are indicated by the different plot symbols. The solid lines are the fitted response functions. For the 0.87μm, 0.66μm and 0.56μm a straight line fit was sufficient, whilst at 1.6μm a third order polynomial was required to obtain a sufficiently good fit. The dashed line in the 1.6μm plot is the linear response extrapolated from low radiance measurements.

7.2 Radiometric Response

After aligning the integrating sphere with the nadir view, the detector gains and offsets were adjusted to get ~ 4000 counts for full sphere output (all lamps on and full aperture), and ~100 counts with the source off. Data were then recorded for all apertures at 390W, 240W, 150W, 90W and 45W lamp settings. A typical result is seen in Figure 7.2, showing the ADC input voltage as a function of sphere radiance for the run with the IR-FPA cooled to 80K.

It was found that the readings from apertures greater than 110mm in diameter gave higher than expected responses. It is not yet known why this has occurred, though it is possible that the path between the UDT radiometer and sphere was partially obstructed for these apertures. Consequentially, these measurements are not used in the analysis. This should not affect the instrument calibration result.

The linearity of the signal channel's response vs. input radiance is defined by first fitting a 2nd order polynomial to the data,

$$V = a_0 + a_1L + a_2L^2. \quad \text{eq. 7.1}$$

The non-linearity at the maximum expected scene radiance is given by the ratio between the linear and non-linear responses

$$\text{Percentage non-linearity} = \frac{a_2L_{\text{max}}}{a_1} \times 100\%. \quad \text{eq. 7.2}$$

	1.6μm	0.87μm	0.66μm	0.56μm
FPA in air	-	0.9%	0.1%	1.5%
FPA in vacuum	-	1.0%	0.4%	1.6%
IR-FPA at 80K	13.4%	1.3%	0.9%	1.1%
Average	13.4%	0.7%	0.5%	1.7%

Table 7-2: Measured non-linearity for AATSR visible channels.

The values for each test case are presented in Table 7-2. The 0.87μm, 0.66μm and 0.56μm channels were linear, i.e. the response was directly proportional to the input radiance. The 1.6μm channel, in contrast, shows a significant decrease in response with increasing radiance. This was a surprising result since it was generally believed that this channel would be linear. It was initially thought that the effect was caused by missing resistors in the pre-amplifier circuit, resulting in the detector being incorrectly biased. However, there was no difference in the result after the resistors were installed. It is therefore likely to be a dR/dV coefficient in the hybrid's high valued feedback resistor.

The radiometric response, α_λ , of the visible channels was obtained by a least squares polynomial fit to the data. For the 0.87μm, 0.66μm and 0.56μm channels a straight line could be

used, Table 7-3. For the 1.6µm a 3rdorder polynomial produced a better-fit, Table 7-4. The normalised residuals from the fitting are shown in Figure 7.3. The errors are summarised in Table 7-5.

	0.87µm	0.66µm	0.56µm
FPA in air	-0.2989	-0.5662	-1.174
FPA in vacuum	-0.3039	-0.5762	-1.181
IR-FPA at 80K	-0.3128	-0.5956	-1.234

Table 7-3: Radiometric responsivity factors, α_λ , mWcm⁻²sr⁻¹V⁻¹, for the 0.87µm, 0.66µm and 0.56µm channels for each test condition.

a ₀	a ₁	a ₂	a ₃
-0.000027	-0.1093	0.009393	0.001013

Table 7-4: Coefficients for converting 1.6µm volts to radiance using $L = a_0 + a_1 V + a_2 V^2 + a_3 V^3$.

Source	1.6µm	0.87µm	0.66µm	0.56µm
Sphere Calibration	8.7%	3.5%	3.3%	3.3%
Error in Fit	0.5%	0.5%	0.5%	0.5%
Repeatability	2.2%	0.5%	0.5%	2.1%
Total RMS Error	9.0%	3.6%	3.4%	3.9%

Table 7-5: Summary of errors in absolute calibration of the AATSR responsivity.

The differences in the responsivities between each test case were repeatable and therefore not due to measurement errors (e.g. repositioning of sphere). This is a genuine effect relating to the operating conditions of the FPA and is similar to in-flight behaviour of ATSR-2 during out-gassing. When the IR-FPA was cooled from ambient to 80K, there would be a decrease in the visible channel signals. The signal recovered when the FPA was warmed up for out-gassing.

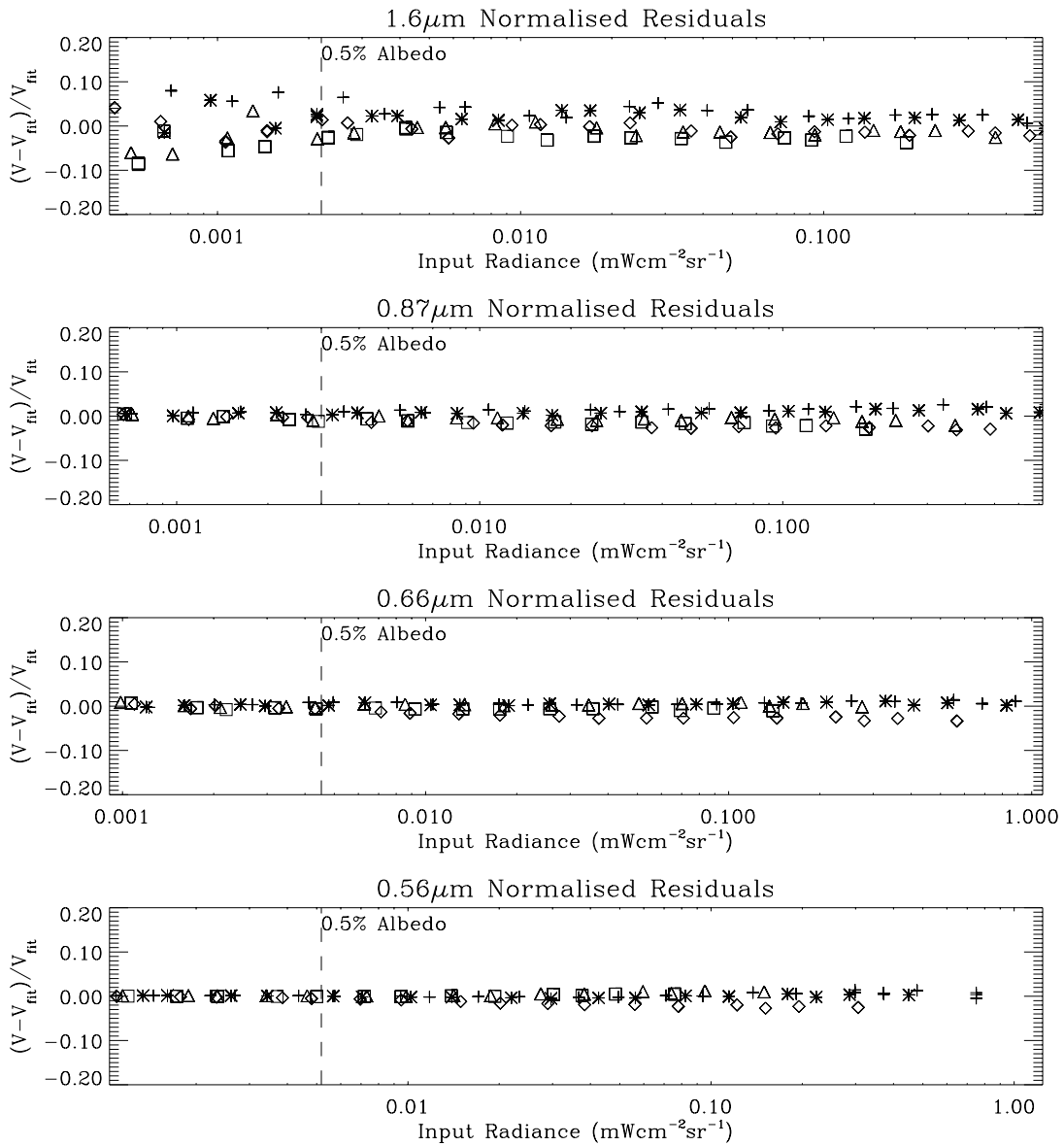
7.3 Radiometric Noise

The instrument performance requirements, AD 1, specify the signal to noise ratio at 0.5% albedo to be at least 20:1. The noise levels measured during this calibration for input radiances corresponding to 0.5% albedo are given in

Table 7-6. All channels met the required specification despite the relatively poor filter transmissions.

Channel	S/N
1.6µm	31:1
0.87µm	25:1
0.66µm	28:1

Table 7-6: Measured signal to noise ratios at 0.5% albedo for AATSR visible channels.



Test : AATSR Visible Calibration - FPA at 80K
File : vis08\$09-oct-1998.le1
Date : 09-OCT-1998 12:27:22.24

Lamp Power
+ 390 W
* 240 W
 \diamond 150 W
 \triangle 90 W
 \square 45 W

Figure 7.3: Normalised residuals from least squares fitting to measured response vs. source radiance.

7.4 VISCAL

7.4.1 Reflectance Factor

The VISCAL reflectance factor, r_{VISCAL} , was measured in a similar way to the responsivity. After aligning the integrating sphere using the method described in §7.1, data were recorded for 390W and 240W lamp settings and apertures down to 12.4 mm diameter. Beyond this, the source did not produce any significant response. The measured detector counts for each channel were converted to scene radiance, L_{scene} , using the calibrations in Table 7-3 and Table 7-4, and plotted against the irradiance at the opal, Figure 7.4. Data for apertures greater than 70mm in diameter were not used because the view to the source from the opal became partially obstructed by the baffle tube. Reflectance factors were obtained by fitting a straight line through the data and multiplying the slope by π . The averages and errors from all the test cases are presented in Table 7-7. The measurements are in excellent agreement with the values calculated from the geometry and optical properties of the system (see §5.1).

	Measured	Expected
1.6 μm	0.191 \pm 0.006	0.192 \pm 0.005
0.87 μm	0.154 \pm 0.003	0.156 \pm 0.004
0.66 μm	0.163 \pm 0.005	0.163 \pm 0.003
0.56 μm	0.163 \pm 0.004	0.165 \pm 0.003

Table 7-7: Measured VISCAL reflectance factors (plus uncertainty) compared against the expected values calculated from the geometry and optical properties

7.4.2 Used Pixels and Uniformity

With the integrating sphere aligned with the VISCAL unit, the scan mirror was run for approximately 10s. While the scan mirror was running, 30 consecutive science data packets were recorded and the pixel counts extracted. For this test, the pixel map was modified so that the range of pixels extended beyond either side of the default VISCAL view (pixel numbers 75 to 90 inclusive). Figure 7.5 shows the average counts, normalised to peak signal, for each pixel over this range. The result shows that the useable pixels from the VISCAL corresponded exactly to the default pixel map and therefore met its specification.

An interesting feature of Figure 7.5 is the slope on the 1.6 μm channel. This is identical to that seen in flight on ATSR-2 (see commissioning report). It was previously believed that the effect was possibly due to stray light from the baffle, but this set of tests suggests a different optical effect that will be discussed later. This should have no significant impact on the instrument calibration since the average of all 16 pixels is used.

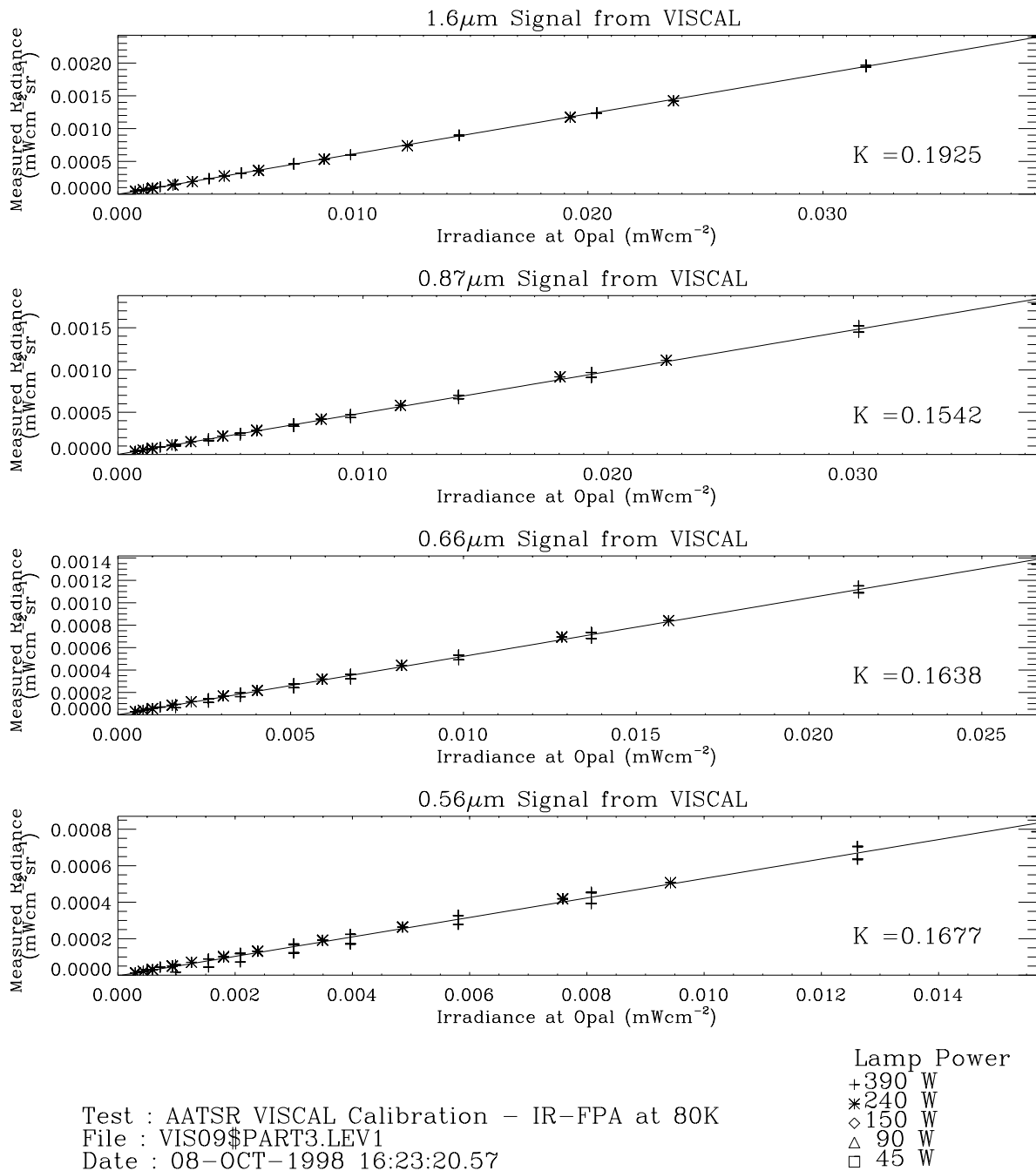


Figure 7.4: Radiance measured from VISCAL unit, versus the irradiance at the opal from the integrating sphere. The data shown here are for the measurements made with the infra-red FPA cooled to 80K.

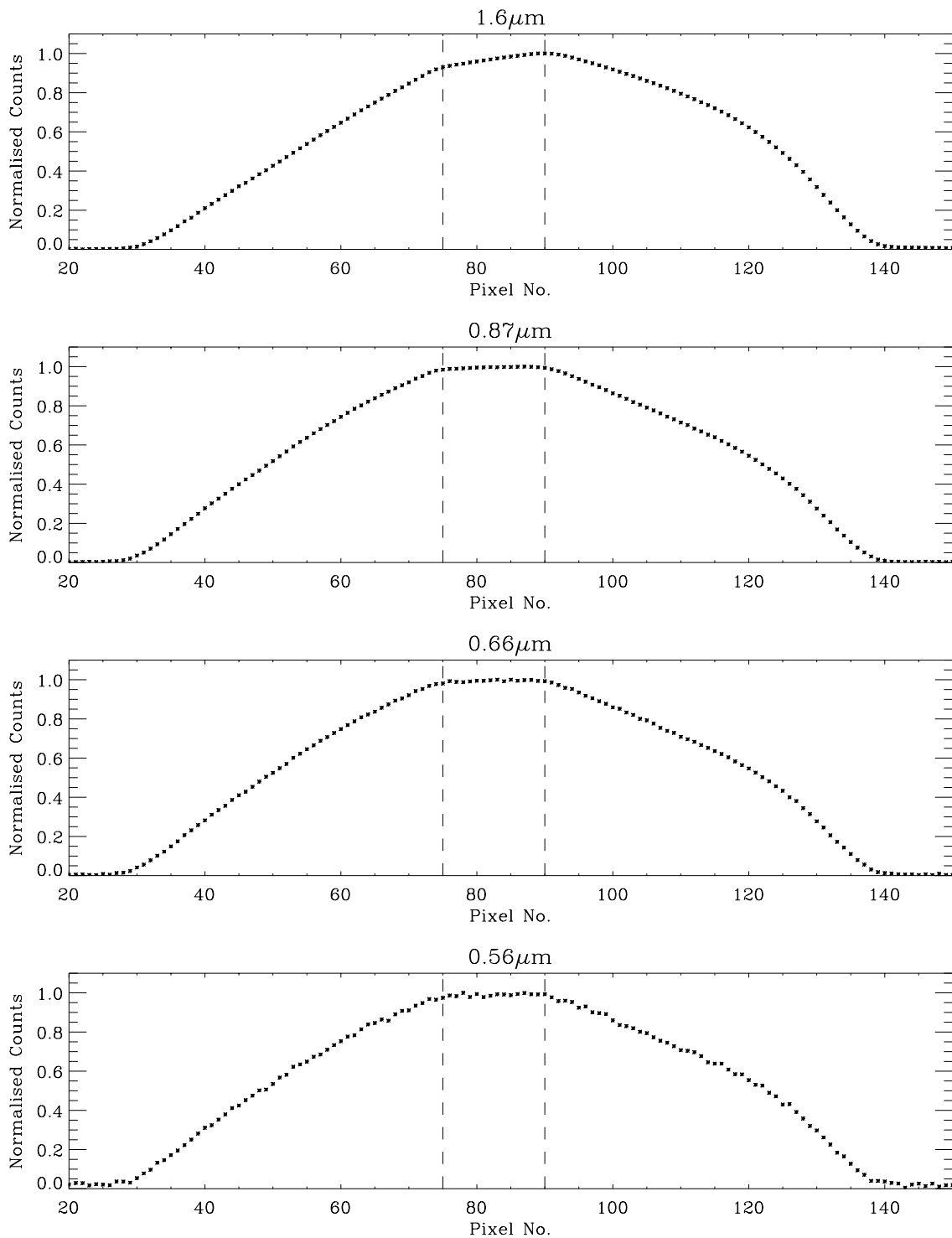
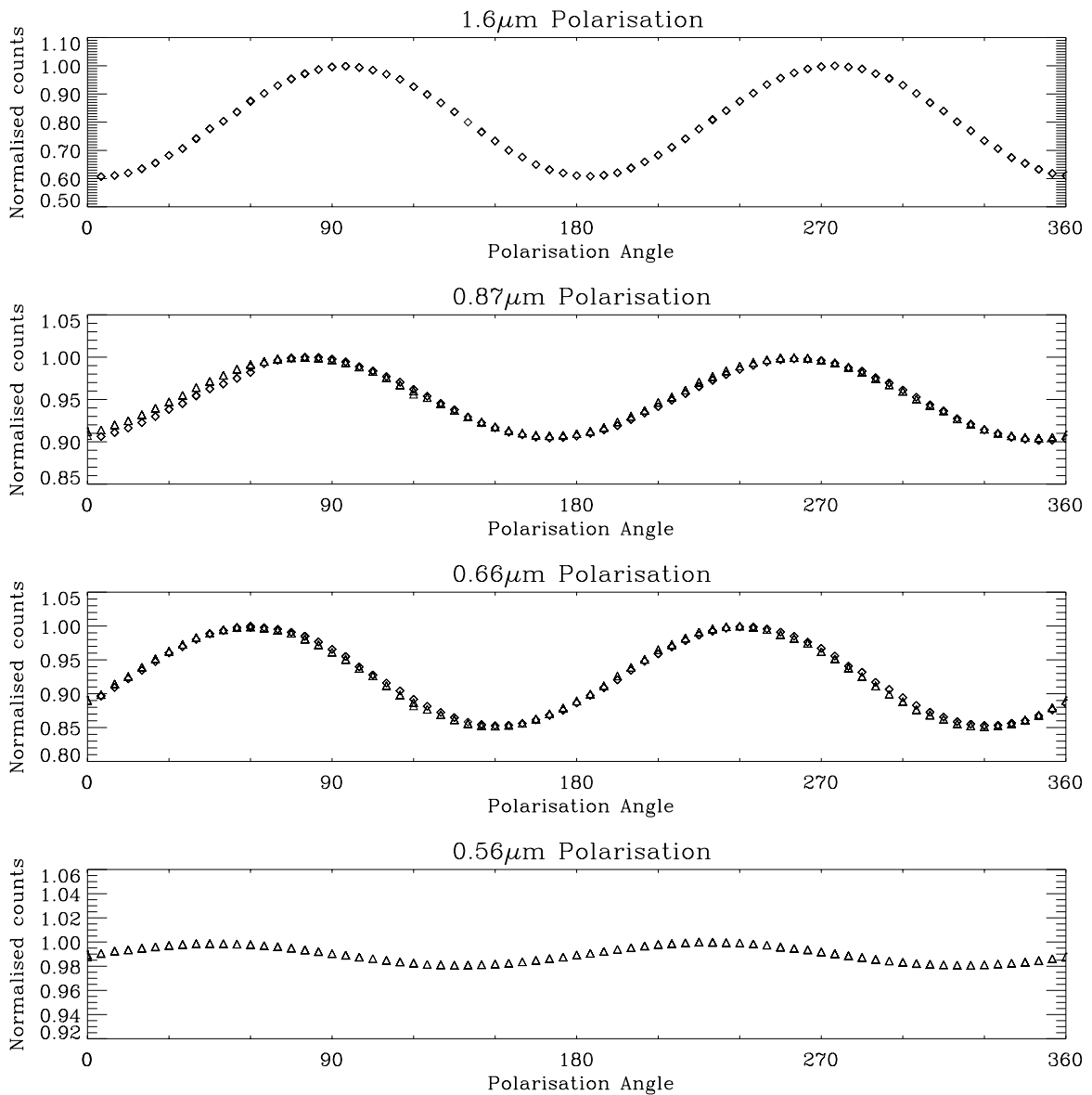


Figure 7.5: Normalised pixel count over the full range of pixels covering the VISCAL. The region bounded by the dashed lines shows where the VISCAL is in full view.

7.5 Polarisation

The large integrating sphere was replaced with the 30W integrating sphere and polarisation filter mounted on an optical bench. The source was aligned with the nadir view in a similar way to the larger source. Data were recorded for both polarisation filters, rotating at 5° intervals in a clockwise direction looking away from the instrument. Measurements were also made with the source blacked out to obtain a background reading. The variations in the measured signals for each channel, normalised to the peak signal, are presented in Figure 7.6.

The maximum variations are 40%, 10%, 15% and 2% for the 1.6µm, 0.87µm, 0.66µm and 0.56µm channels respectively. The data for the 0.87µm and 0.66µm were repeated exactly for both polarisation filters. The magnitude of the polarisation variation is in good agreement with the unit level measurements made by AUSPACE. A difference being with the 0.87µm channel, which appears to be slightly more sensitive to polarisation in the instrument level tests.



Test : AATSR Visible Calibration – Polarisation Sensitivity
File : vis07\$02-NOV-1997.LEV1
Date : 02-NOV-1997 16:19:52.56
◇ Ealing Optics IR polariser
△ Ealing Optics Visible polariser

Figure 7.6: Normalised response as a function of polarisation angle.

7.6 Scan dependent effects

To investigate if there are any scan dependent effects in the visible calibration, data were recorded with the large integrating sphere positioned at the centres and ends of the Nadir and Along-Track baffles. The measurements were made using the 240W lamp setting and the 100mm aperture so that none of the channels would go over range. The measured response, normalised to the average for all positions, Figure 7.7, shows a maximum deviation of around 1%. This is most likely to be due to errors in aligning the integrating sphere with the instrument.

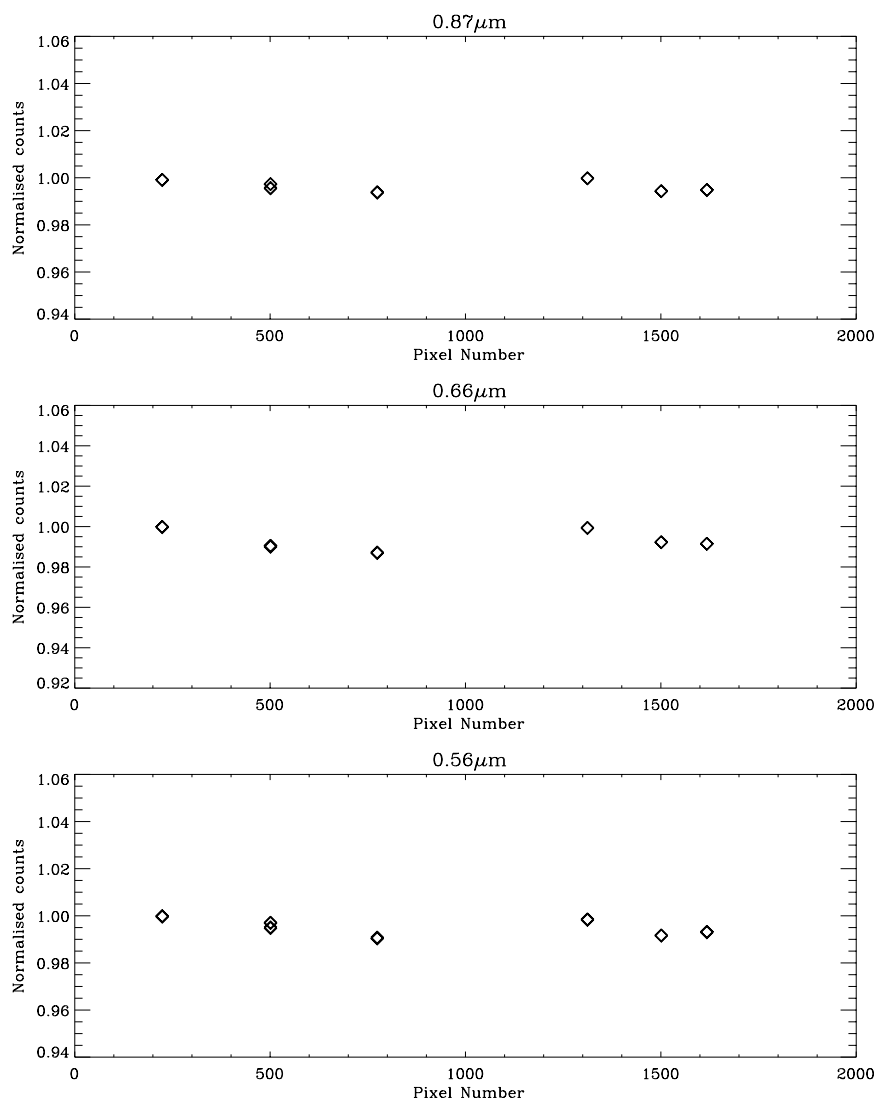


Figure 7.7: Normalised visible channel responses for constant integrating sphere illumination, against approximate pixel position around scan.

7.7 Uniformity of response across aperture.

An additional test was performed to measure the variation in the radiometric response across the instrument aperture. Using an 8mm aperture, the large integrating sphere was scanned both horizontally and vertically across the field-of-view, and the pixel counts recorded for each position. The IR FPA was cooled to 80K for this test so data for the 1.6 μ m channel were also recorded.

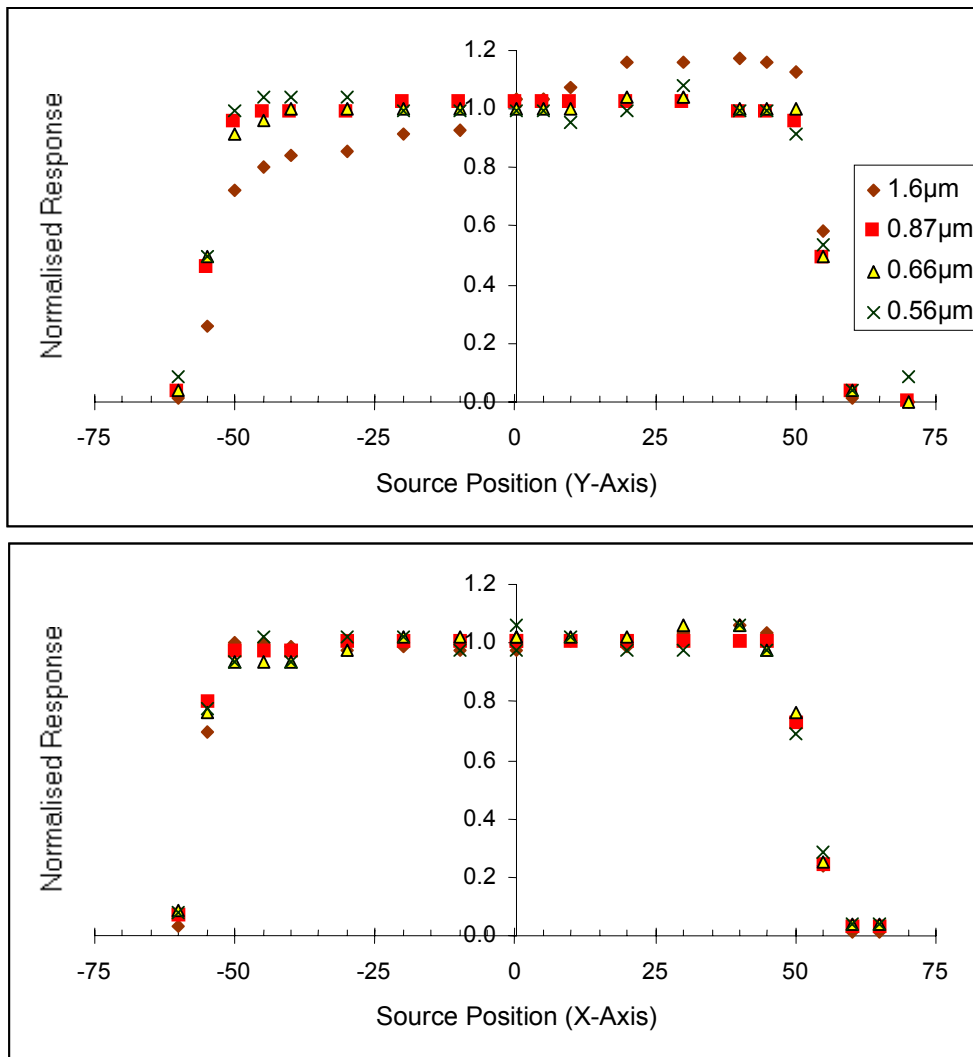


Figure 7.8: Visible channel responses, normalised to average signal, for 8mm diffuse source scanned across the nadir aperture horizontally (instrument y-axis) and vertically (instrument x-axis).

The results in Figure 7.8 show the 1.6 μ m channel response to vary significantly across the horizontal axes (instrument y-axis). The response varies by up to 40% from one edge of the aperture to the other. The other channels do not exhibit this, and no effect is seen in the vertical

axis (instrument x-axis). This means that the signal measured by the detector will be dependent on what part of the aperture is illuminated. The variation across the instrument aperture is caused because the position on the aperture is correlated with the angle of incidence on beam-splitter 4 in the IR-FPA. This component has a spectral edge that interacts with the 1.6 μ m channel, whose position depends on the angle of incidence.

The effect may be related to the non-linear radiometric response of the 1.6 μ m channel (Figure 7.2) and, the variation across the VISCAL at this wavelength (Figure 7.5). This will not apply to the in-flight pixel data, since the radiation from a distant point source will uniformly fill the full aperture.

The VISCAL unit was designed to give the maximum possible signal within practical constraints. To give a signal corresponding to approximately 15% surface reflectance for 16 consecutive pixels, required the source to be smaller than the main instrument aperture. During the calibration period, the uniformly illuminated source is scanned across the off-axis-parabolic mirror. Because of the non-uniform response across the aperture, the measured signal from the source will also change with pixel number. The magnitude of this being dependent on the direction the source is scanned.

For the absolute radiometric calibration, the input flux was controlled by varying the source aperture diameter. It is therefore possible that the measured signal would not vary linearly with source aperture area. However, for these measurements, the scan mirror was stationary and the centre of the source was fixed. Therefore, if the centre of the source were aligned with the centre of the aperture, the measured response would be the average for a series of measurements taken over the whole aperture. This is confirmed in Figure 7.8, which shows the normalised response of the central pixel in the y-axis direction to be 1.0. Another confirmation is seen in Figure 7.2 and Figure 7.3 that show exactly the same result with runs at different lamp settings.

8 Summary and Conclusions

The in-flight calibration of the AATSR visible channels depends on the radiometric response for each channel, α , and the VISCAL reflectance factor, r_{VISCAL} , §5. These parameters have been measured for all AATSR visible channels using a Labsphere 2000 integrating sphere calibrated at NPL to <3.5% absolute accuracy for wavelengths up to 1 μm and 8.7% accuracy at 1.6 μm .

The test results showed that the 0.87 μm , 0.66 μm and 0.56 μm were linear with input radiance. The radiometric responses for these channels under different conditions are given in Table 7-3. At the start of the AATSR mission the values of α used should correspond to a clean FPA in vacuo with the IR-FPA at ambient temperature.

The 1.6 μm channel was found to have a significantly non-linear radiometric response (13.4% for radiances corresponding to full albedo). This has been quantified, and a calibration algorithm has been derived for the ground-segment processing (Appendix B).

The reflectance factor of the VISCAL unit was measured for all channels and was found to be in excellent agreement with prediction, Table 7-7. An interesting result was the 10% variation of signal across the VISCAL unit at 1.6 μm channel, Figure 7.5. This was very similar to the in-flight data from ATSR-2. This effect is not due to the properties of the VISCAL itself, but rather caused by non-uniform response across the main aperture, and will not affect the calibration of this channel in-flight integrated across the full aperture.

A summary of the calibration errors and signal/noise levels is given in Table 8-1.

	1.6 μm	0.87 μm	0.66 μm	0.56 μm
Error in radiometric response	9.0%	3.6%	3.4%	3.9%
Error in VISCAL reflectance factor	3.3%	2.0%	3.2%	2.4%
S/N at 0.5% albedo	31:1	25:1	28:1	25:1

Table 8-1: Visible Channel calibration errors and radiometric noise. The signal to noise requirement stated in AD 1 is 20:1 at 0.5% albedo.

Variations in the radiometric calibration around the scan cone were < 1%. It is likely that the observed variations were caused by inaccuracy in positioning the source.

The sensitivity to polarisation at the centre of nadir-view was also measured for all channels. The maximum variations in signal channel responses were found to be 40%, 10%, 15% and 2% for the 1.6 μm , 0.87 μm , 0.66 μm and 0.56 μm channels respectively. The 1.6 μm value is above specification but accepted because it has been quantified.

To conclude, the visible channels meet the performance requirements specified in AD 1. In addition, the calibration has revealed critical information on the 1.6 μm channel that benefit both AATSR and ATSR-2 calibrations. To obtain the full benefit of this calibration, it is recommended that further spot measurements be performed before launch. These will identify

any drifts in calibration that could occur because of mechanical movements or contamination of the optical components, and allow any necessary corrections to be made.

Appendix A Test Plan Summary

Test No	Test Title	Description of Test
VIS01	Integrating Sphere Calibration	Calibrate output of integrating sphere for full range of power settings and aperture diameters.
VIS02	Visible Radiometric Calibration	Measure detector response as a function of input radiance at the centre of nadir view for full range of integrating sphere lamp settings and aperture diameters.
VIS03	A/D Linearity Test	Change detector gains and offsets and verify calibration using a reduced set of input levels.
VIS04	Scan Dependent Effects	Verify calibration at different points around the scan cone using full illumination.
VIS05	VISCAL Calibration	Position the scan mirror so that the beam is in the direction of the VISCAL unit. Measure detector counts vs. input illumination.
VIS06	VISCAL Viewed Pixels	With the integrating sphere output set to maximum intensity, run the scan mirror for a few seconds and record the VISCAL pixel counts.
VIS07	Polarisation Sensitivity	Measure the variation in the detector response as a function of polarisation angle.
VIS08	Repeat Visible Radiometric Calibration	Measure detector response as a function of input radiance at the centre of nadir view for full range of integrating sphere lamp settings and aperture diameters.
VIS09	Repeat VISCAL Calibration	Position the scan mirror so that the beam is in the direction of the VISCAL unit. Measure detector counts vs. input illumination.

Appendix B 1.6µm Calibration

This calibration has revealed that the 1.6µm channel was significantly non-linear. Consequentially the in-flight calibration method applied to the other, more linear, visible channels can be no longer used. Here the measured signal for a given scene, V_{scene} may be converted to a reflectance, r_{scene} using

$$r_{scene} = r_{viscal} V_{scene} / V_{VISCAL} \quad B.1$$

where r_{viscal} and V_{dark} are the VISCAL reflectance factor and ADC input volts. It is assumed that the dark counts have been subtracted and the result is normalised to unit gain.

For the 1.6µm calibration the normalised counts have to be converted to a scene reflectance using the absolute calibration results

$$r_{scene} = \pi L_{scene} / I_0 = \pi (a_0 + a_1 V + a_2 V^2 + a_3 V^3) / I_0. \quad B.2$$

where $a_0 = -0.000027$, $a_1 = -0.1093$, $a_2 = 0.009393$ and $a_3 = 0.001013$, and I_0 is the solar spectral irradiance at 1.6µm = 1.553mWcm⁻².

In practice the conversion from counts to reflectance may be done using a look-up-table consisting of 100 points presented in this appendix.

However, the pre-launch absolute calibration will not provide any compensation for changes in the primary optical performance. After several months in orbit the signal reaching the detector will have degraded by a factor D so that

$$r_{true} = r(V_{meas}) / D. \quad B.3$$

For ATSR-2 this was found to be about 0.4% per year at 1.6µm. Since the VISCAL unit gives a known signal corresponding to a reflectance, r_{viscal} , the drift can be obtained using

$$D = r(V_{VISCAL}) / r_{VISCAL}. \quad B.4$$

Substituting 4 into 3 gives

$$r_{scene} = r_{viscal} r(V_{scene}) / r(V_{VISCAL}) \quad B.5$$

which is identical in form to equation 1. So, in principle the software changes for the 1.6µm calibration could be kept to a minimum. In addition there are no technical reasons why the same method could not be applied for all the visible channels.

1.6µm conversion from normalised counts to reflectance

Normalised Counts	ADC Volts	Irradiance mWcm ⁻² sr ⁻¹	Reflectance
0.00	0.00	0.000	0.000
0.30	-0.06	0.007	0.013
0.60	-0.12	0.013	0.027
0.90	-0.18	0.020	0.040
1.20	-0.24	0.027	0.054
1.50	-0.30	0.034	0.068
1.80	-0.36	0.040	0.082
2.10	-0.42	0.047	0.096
2.40	-0.48	0.054	0.110
2.70	-0.54	0.062	0.125
3.00	-0.60	0.069	0.139
3.30	-0.66	0.076	0.154
3.60	-0.72	0.083	0.168
3.90	-0.78	0.090	0.183
4.20	-0.84	0.098	0.198
4.50	-0.90	0.105	0.213
4.80	-0.96	0.113	0.228
5.10	-1.02	0.120	0.243
5.40	-1.08	0.128	0.258
5.70	-1.14	0.135	0.274
6.00	-1.20	0.143	0.289
6.30	-1.26	0.151	0.305
6.60	-1.32	0.158	0.320
6.90	-1.38	0.166	0.336
7.20	-1.44	0.174	0.352
7.50	-1.50	0.182	0.367
7.80	-1.56	0.190	0.383
8.10	-1.62	0.197	0.399
8.40	-1.68	0.205	0.415
8.70	-1.74	0.213	0.431
9.00	-1.80	0.221	0.448
9.30	-1.86	0.229	0.464
9.60	-1.92	0.237	0.480
9.90	-1.98	0.245	0.496
10.20	-2.04	0.253	0.513
10.50	-2.10	0.262	0.529
10.80	-2.16	0.270	0.546
11.10	-2.22	0.278	0.562
11.40	-2.28	0.286	0.579
11.70	-2.34	0.294	0.595
12.00	-2.40	0.302	0.612
12.30	-2.46	0.311	0.628

Normalised Counts	ADC Volts	Irradiance mWcm ⁻² sr ⁻¹	Reflectance
12.60	-2.52	0.319	0.645
12.90	-2.58	0.327	0.662
13.20	-2.64	0.335	0.678
13.50	-2.70	0.344	0.695
13.80	-2.76	0.352	0.712
14.10	-2.82	0.360	0.729
14.40	-2.88	0.368	0.745
14.70	-2.94	0.377	0.762
15.00	-3.00	0.385	0.779
15.30	-3.06	0.393	0.796
15.60	-3.12	0.402	0.813
15.90	-3.18	0.410	0.829
16.20	-3.24	0.418	0.846
16.50	-3.30	0.427	0.863
16.80	-3.36	0.435	0.880
17.10	-3.42	0.443	0.896
17.40	-3.48	0.451	0.913
17.70	-3.54	0.460	0.930
18.00	-3.60	0.468	0.947
18.30	-3.66	0.476	0.963
18.60	-3.72	0.484	0.980
18.90	-3.78	0.493	0.997
19.20	-3.84	0.501	1.013
19.50	-3.90	0.509	1.030
19.80	-3.96	0.517	1.046
20.10	-4.02	0.525	1.063
20.40	-4.08	0.534	1.079
20.70	-4.14	0.542	1.096
21.00	-4.20	0.550	1.112
21.30	-4.26	0.558	1.128
21.60	-4.32	0.566	1.145
21.90	-4.38	0.574	1.161
22.20	-4.44	0.582	1.177
22.50	-4.50	0.590	1.193
22.80	-4.56	0.598	1.209
23.10	-4.62	0.606	1.225
23.40	-4.68	0.613	1.241
23.70	-4.74	0.621	1.257
24.00	-4.80	0.629	1.273
24.30	-4.86	0.637	1.288
24.60	-4.92	0.645	1.304
24.90	-4.98	0.652	1.319
25.20	-5.04	0.660	1.335
25.50	-5.10	0.667	1.350
25.80	-5.16	0.675	1.365

Normalised Counts	ADC Volts	Irradiance $\text{mWcm}^{-2}\text{sr}^{-1}$	Reflectance
26.10	-5.22	0.682	1.380
26.40	-5.28	0.690	1.396
26.70	-5.34	0.697	1.411
27.00	-5.40	0.705	1.425
27.30	-5.46	0.712	1.440
27.60	-5.52	0.719	1.455
27.90	-5.58	0.726	1.469
28.20	-5.64	0.734	1.484
28.50	-5.70	0.741	1.498
28.80	-5.76	0.748	1.512
29.10	-5.82	0.755	1.527
29.40	-5.88	0.762	1.541
29.70	-5.94	0.768	1.554
30.00	-6.00	0.775	1.568

Appendix C Visible Channel Spectral Response

1.6µm

Wavelength Response µm	Wavelength Response µm	Wavelength Response µm	Wavelength Response µm
1.447824	0.00001	1.502147	0.00095
1.449117	0.00001	1.503441	0.00108
1.450410	0.00001	1.504734	0.00110
1.451704	0.00001	1.506027	0.00119
1.452997	0.00000	1.507321	0.00143
1.454291	0.00000	1.508614	0.00152
1.455584	0.00000	1.509908	0.00177
1.456878	0.00000	1.511201	0.00188
1.458171	0.00000	1.512495	0.00210
1.459464	0.00000	1.513788	0.00239
1.460758	0.00000	1.515081	0.00253
1.462051	0.00000	1.516375	0.00277
1.463345	0.00000	1.517668	0.00319
1.464638	0.00000	1.518962	0.00357
1.465931	0.00000	1.520255	0.00387
1.467225	0.00000	1.521549	0.00449
1.468518	0.00000	1.522842	0.00494
1.469812	0.00000	1.524135	0.00573
1.471105	0.00001	1.525429	0.00638
1.472399	0.00000	1.526722	0.00741
1.473692	0.00001	1.528016	0.00852
1.474985	0.00001	1.529309	0.00989
1.476279	0.00002	1.530602	0.01171
1.477572	0.00003	1.531896	0.01381
1.478866	0.00005	1.533189	0.01649
1.480159	0.00007	1.534483	0.01957
1.481453	0.00010	1.535776	0.02350
1.482746	0.00010	1.537070	0.02826
1.484039	0.00014	1.538363	0.03387
1.485333	0.00017	1.539656	0.04111
1.486626	0.00017	1.540950	0.05009
1.487920	0.00018	1.542243	0.06101
1.489213	0.00018	1.543537	0.07446
1.490506	0.00020	1.544830	0.09107
1.491800	0.00029	1.546124	0.11047
1.493093	0.00045	1.547417	0.13143
1.494387	0.00067	1.548710	0.15509
1.495680	0.00073	1.550004	0.18169
1.496974	0.00073	1.551297	0.21050
1.498267	0.00076	1.552591	0.24100
1.499560	0.00085	1.553884	0.27164
1.500854	0.00092	1.555177	0.30122
		1.556471	0.33446
		1.557764	0.36986
		1.559058	0.40497
		1.560351	0.44161
		1.561645	0.47867
		1.562938	0.51617
		1.564231	0.55151
		1.565525	0.58882
		1.566818	0.62886
		1.568112	0.66566
		1.569405	0.70495
		1.570698	0.74698
		1.571992	0.78266
		1.573285	0.81873
		1.574579	0.85700
		1.575872	0.88899
		1.577166	0.91736
		1.578459	0.94384
		1.579752	0.96339
		1.581046	0.97886
		1.582339	0.99052
		1.583633	0.99534
		1.584926	0.99935
		1.586220	0.99997
		1.587513	0.99874
		1.588806	1.00000
		1.590100	0.99492
		1.591393	0.98939
		1.592687	0.98500
		1.593980	0.98067
		1.595273	0.97274
		1.596567	0.96300
		1.597860	0.95380
		1.599154	0.94267
		1.600447	0.93150
		1.601741	0.91502
		1.603034	0.89402
		1.604327	0.87956
		1.605621	0.86260
		1.606914	0.84387
		1.608208	0.82207
		1.609501	0.80038
		1.610794	0.78011
		1.612088	0.76009
		1.613381	0.73700
		1.614675	0.71177
		1.615968	0.68754
		1.617262	0.66412
		1.618555	0.63725
		1.619848	0.61077
		1.621142	0.58320
		1.622435	0.55455
		1.623729	0.52648
		1.625022	0.49739
		1.626316	0.46646
		1.627609	0.43473
		1.628902	0.40106
		1.630196	0.36762
		1.631489	0.33449
		1.632783	0.30209
		1.634076	0.27078
		1.635369	0.23981
		1.636663	0.21227
		1.637956	0.18632
		1.639250	0.16149
		1.640543	0.13890
		1.641837	0.11880
		1.643130	0.10048
		1.644423	0.08514
		1.645717	0.07215
		1.647010	0.06122
		1.648304	0.05226
		1.649597	0.04460
		1.650891	0.03803
		1.652184	0.03271
		1.653477	0.02857
		1.654771	0.02490
		1.656064	0.02191
		1.657358	0.01922
		1.658651	0.01697
		1.659944	0.01507
		1.661238	0.01328
		1.662531	0.01183
		1.663825	0.01075

<u>Wavelength Response</u> <u>μm</u>		<u>Wavelength Response</u> <u>μm</u>		<u>Wavelength Response</u> <u>μm</u>		<u>Wavelength Response</u> <u>μm</u>	
1.665118	0.00974	1.693573	0.00156	1.722029	0.00040	1.750484	0.00026
1.666412	0.00875	1.694867	0.00150	1.723322	0.00034	1.751777	0.00026
1.667705	0.00797	1.696160	0.00142	1.724615	0.00031	1.753071	0.00026
1.668998	0.00712	1.697454	0.00132	1.725909	0.00030	1.754364	0.00026
1.670292	0.00649	1.698747	0.00128	1.727202	0.00027	1.755658	0.00027
1.671585	0.00604	1.700040	0.00127	1.728496	0.00025	1.756951	0.00027
1.672879	0.00539	1.701334	0.00125	1.729789	0.00024	1.758244	0.00027
1.674172	0.00504	1.702627	0.00117	1.731083	0.00024	1.759538	0.00027
1.675465	0.00468	1.703921	0.00095	1.732376	0.00024	1.760831	0.00027
1.676759	0.00432	1.705214	0.00080	1.733669	0.00024	1.762125	0.00028
1.678052	0.00388	1.706508	0.00067	1.734963	0.00023	1.763418	0.00028
1.679346	0.00360	1.707801	0.00053	1.736256	0.00024	1.764711	0.00028
1.680639	0.00331	1.709094	0.00050	1.737550	0.00024	1.766005	0.00028
1.681933	0.00301	1.710388	0.00049	1.738843	0.00024	1.767298	0.00028
1.683226	0.00283	1.711681	0.00048	1.740137	0.00024	1.768592	0.00028
1.684519	0.00271	1.712975	0.00048	1.741430	0.00024	1.769885	0.00029
1.685813	0.00241	1.714268	0.00047	1.742723	0.00024	1.771179	0.00029
1.687106	0.00224	1.715562	0.00048	1.744017	0.00025	1.772472	0.00029
1.688400	0.00205	1.716855	0.00047	1.745310	0.00025	1.773765	0.00029
1.689693	0.00181	1.718148	0.00045	1.746604	0.00025	1.775059	0.00028
1.690987	0.00177	1.719442	0.00043	1.747897	0.00025	1.776352	0.00030
1.692280	0.00169	1.720735	0.00042	1.749190	0.00025		

0.87µm

Wavelength µm	Response	Wavelength µm	Response	Wavelength µm	Response	Wavelength µm	Response
0.834274	0.00092	0.846204	0.03184	0.858134	0.89337	0.870064	0.77541
0.834533	0.00097	0.846463	0.03579	0.858393	0.88466	0.870323	0.74381
0.834792	0.00101	0.846722	0.03994	0.858653	0.87639	0.870583	0.71035
0.835052	0.00103	0.846982	0.04485	0.858912	0.87264	0.870842	0.67546
0.835311	0.00111	0.847241	0.05043	0.859171	0.86813	0.871101	0.64194
0.835570	0.00125	0.847500	0.05726	0.859431	0.86265	0.871361	0.60493
0.835830	0.00134	0.847760	0.06518	0.859690	0.85794	0.871620	0.57224
0.836089	0.00149	0.848019	0.07410	0.859949	0.86013	0.871879	0.53843
0.836348	0.00153	0.848279	0.08408	0.860209	0.86102	0.872139	0.50456
0.836608	0.00164	0.848538	0.09591	0.860468	0.85899	0.872398	0.46906
0.836867	0.00166	0.848797	0.10951	0.860727	0.86062	0.872657	0.43539
0.837126	0.00182	0.849057	0.12488	0.860987	0.86461	0.872917	0.40388
0.837386	0.00205	0.849316	0.14182	0.861246	0.86792	0.873176	0.37146
0.837645	0.00208	0.849575	0.16092	0.861505	0.87355	0.873435	0.34066
0.837905	0.00219	0.849835	0.18299	0.861765	0.87900	0.873695	0.31402
0.838164	0.00235	0.850094	0.20971	0.862024	0.88338	0.873954	0.28727
0.838423	0.00244	0.850353	0.23809	0.862283	0.89123	0.874214	0.26452
0.838683	0.00279	0.850613	0.27049	0.862543	0.89767	0.874473	0.24412
0.838942	0.00300	0.850872	0.30613	0.862802	0.90770	0.874732	0.22416
0.839201	0.00319	0.851131	0.34426	0.863061	0.91500	0.874992	0.20374
0.839461	0.00335	0.851391	0.38585	0.863321	0.92185	0.875251	0.18577
0.839720	0.00350	0.851650	0.43182	0.863580	0.93279	0.875510	0.17016
0.839979	0.00380	0.851909	0.47719	0.863840	0.94239	0.875770	0.15676
0.840239	0.00423	0.852169	0.52326	0.864099	0.95215	0.876029	0.14393
0.840498	0.00458	0.852428	0.57208	0.864358	0.96235	0.876288	0.13177
0.840757	0.00488	0.852687	0.61951	0.864618	0.97048	0.876548	0.11983
0.841017	0.00527	0.852947	0.66247	0.864877	0.98116	0.876807	0.10903
0.841276	0.00563	0.853206	0.70792	0.865136	0.98873	0.877066	0.10047
0.841535	0.00611	0.853466	0.75085	0.865396	0.99220	0.877326	0.09350
0.841795	0.00661	0.853725	0.79029	0.865655	0.99393	0.877585	0.08614
0.842054	0.00729	0.853984	0.83135	0.865914	0.99749	0.877844	0.07913
0.842313	0.00780	0.854244	0.86875	0.866174	0.99783	0.878104	0.07357
0.842573	0.00844	0.854503	0.89242	0.866433	1.00000	0.878363	0.06854
0.842832	0.00907	0.854762	0.92018	0.866692	0.99420	0.878622	0.06330
0.843092	0.00998	0.855022	0.94016	0.866952	0.99329	0.878882	0.05890
0.843351	0.01105	0.855281	0.94893	0.867211	0.98929	0.879141	0.05524
0.843610	0.01198	0.855540	0.95445	0.867470	0.97812	0.879401	0.05102
0.843870	0.01310	0.855800	0.95825	0.867730	0.96401	0.879660	0.04648
0.844129	0.01425	0.856059	0.95716	0.867989	0.95227	0.879919	0.04336
0.844388	0.01577	0.856318	0.95313	0.868248	0.93624	0.880179	0.04087
0.844648	0.01721	0.856578	0.94532	0.868508	0.92097	0.880438	0.03756
0.844907	0.01888	0.856837	0.93834	0.868767	0.90245	0.880697	0.03453
0.845166	0.02089	0.857096	0.92823	0.869027	0.88199	0.880957	0.03265
0.845426	0.02324	0.857356	0.92095	0.869286	0.85687	0.881216	0.03065
0.845685	0.02585	0.857615	0.91082	0.869545	0.82950	0.881475	0.02795
0.845944	0.02856	0.857874	0.89836	0.869805	0.80426	0.881735	0.02632

<u>Wavelength Response</u> <u>μm</u>		<u>Wavelength Response</u> <u>μm</u>		<u>Wavelength Response</u> <u>μm</u>		<u>Wavelength Response</u> <u>μm</u>	
0.881994	0.02499	0.886662	0.00800	0.891331	0.00264	0.895999	0.00077
0.882253	0.02310	0.886922	0.00728	0.891590	0.00241	0.896258	0.00075
0.882513	0.02155	0.887181	0.00700	0.891849	0.00225	0.896518	0.00056
0.882772	0.02065	0.887440	0.00674	0.892109	0.00215	0.896777	0.00053
0.883031	0.01914	0.887700	0.00629	0.892368	0.00199	0.897036	0.00038
0.883291	0.01765	0.887959	0.00598	0.892627	0.00194	0.897296	0.00039
0.883550	0.01677	0.888218	0.00565	0.892887	0.00180	0.897555	0.00033
0.883809	0.01586	0.888478	0.00525	0.893146	0.00163	0.897814	0.00031
0.884069	0.01457	0.888737	0.00491	0.893405	0.00150	0.898074	0.00026
0.884328	0.01385	0.888996	0.00465	0.893665	0.00140	0.898333	0.00025
0.884588	0.01318	0.889256	0.00431	0.893924	0.00135	0.898592	0.00023
0.884847	0.01223	0.889515	0.00415	0.894183	0.00123	0.898852	0.00016
0.885106	0.01130	0.889775	0.00385	0.894443	0.00111	0.899111	0.00013
0.885366	0.01074	0.890034	0.00363	0.894702	0.00106	0.899370	0.00017
0.885625	0.01021	0.890293	0.00335	0.894962	0.00098	0.899630	0.00010
0.885884	0.00952	0.890553	0.00307	0.895221	0.00095	0.899889	0.00001
0.886144	0.00897	0.890812	0.00292	0.895480	0.00087	0.900149	0.00000
0.886403	0.00865	0.891071	0.00272	0.895740	0.00080		

0.66µm

Wavelength µm	Response	Wavelength µm	Response	Wavelength µm	Response	Wavelength µm	Response
0.629289	0.00000	0.641235	0.02077	0.653180	0.79392	0.665125	0.89028
0.629549	0.00001	0.641494	0.02293	0.653440	0.80825	0.665385	0.88368
0.629809	0.00003	0.641754	0.02518	0.653699	0.82689	0.665645	0.87385
0.630068	0.00009	0.642014	0.02793	0.653959	0.84214	0.665904	0.86464
0.630328	0.00021	0.642273	0.03134	0.654219	0.85312	0.666164	0.85302
0.630588	0.00034	0.642533	0.03470	0.654478	0.87056	0.666424	0.83907
0.630847	0.00042	0.642793	0.03864	0.654738	0.88013	0.666683	0.82434
0.631107	0.00051	0.643052	0.04313	0.654998	0.89568	0.666943	0.80813
0.631367	0.00067	0.643312	0.04835	0.655257	0.90863	0.667203	0.78836
0.631626	0.00058	0.643572	0.05393	0.655517	0.91931	0.667462	0.76657
0.631886	0.00072	0.643831	0.06026	0.655777	0.92943	0.667722	0.74592
0.632146	0.00089	0.644091	0.06707	0.656036	0.94287	0.667982	0.71919
0.632405	0.00101	0.644351	0.07489	0.656296	0.95232	0.668241	0.68978
0.632665	0.00112	0.644610	0.08395	0.656556	0.96241	0.668501	0.66060
0.632925	0.00116	0.644870	0.09315	0.656815	0.97159	0.668761	0.62891
0.633185	0.00130	0.645130	0.10392	0.657075	0.97711	0.669020	0.59768
0.633444	0.00160	0.645389	0.11581	0.657335	0.98220	0.669280	0.56704
0.633704	0.00179	0.645649	0.12813	0.657594	0.98560	0.669540	0.53294
0.633964	0.00191	0.645909	0.14275	0.657854	0.99326	0.669799	0.50115
0.634223	0.00205	0.646169	0.15755	0.658114	0.99349	0.670059	0.46868
0.634483	0.00223	0.646428	0.17432	0.658373	0.99731	0.670319	0.43685
0.634743	0.00233	0.646688	0.19208	0.658633	0.99961	0.670578	0.40628
0.635002	0.00257	0.646948	0.21188	0.658893	0.99981	0.670838	0.37381
0.635262	0.00270	0.647207	0.23045	0.659153	1.00000	0.671098	0.34596
0.635522	0.00317	0.647467	0.25370	0.659412	0.99628	0.671357	0.31746
0.635781	0.00344	0.647727	0.27831	0.659672	0.99543	0.671617	0.29087
0.636041	0.00368	0.647986	0.30596	0.659932	0.99232	0.671877	0.26639
0.636301	0.00412	0.648246	0.32921	0.660191	0.99422	0.672137	0.24380
0.636560	0.00442	0.648506	0.35895	0.660451	0.98959	0.672396	0.22156
0.636820	0.00468	0.648765	0.38716	0.660711	0.98451	0.672656	0.20271
0.637080	0.00515	0.649025	0.41832	0.660970	0.97942	0.672916	0.18387
0.637339	0.00563	0.649285	0.44847	0.661230	0.97636	0.673175	0.16866
0.637599	0.00596	0.649544	0.48226	0.661490	0.97270	0.673435	0.15268
0.637859	0.00653	0.649804	0.51087	0.661749	0.96509	0.673695	0.13997
0.638118	0.00701	0.650064	0.53991	0.662009	0.96218	0.673954	0.12734
0.638378	0.00750	0.650323	0.56766	0.662269	0.95949	0.674214	0.11622
0.638638	0.00812	0.650583	0.59197	0.662528	0.95265	0.674474	0.10560
0.638897	0.00890	0.650843	0.61512	0.662788	0.94508	0.674733	0.09684
0.639157	0.00980	0.651102	0.63926	0.663048	0.93997	0.674993	0.08884
0.639417	0.01066	0.651362	0.66095	0.663307	0.93108	0.675253	0.08162
0.639677	0.01168	0.651622	0.68246	0.663567	0.92955	0.675512	0.07536
0.639936	0.01272	0.651881	0.70140	0.663827	0.92275	0.675772	0.06941
0.640196	0.01400	0.652141	0.71982	0.664086	0.91927	0.676032	0.06453
0.640456	0.01547	0.652401	0.74128	0.664346	0.91174	0.676291	0.05964
0.640715	0.01687	0.652661	0.75814	0.664606	0.90703	0.676551	0.05519
0.640975	0.01862	0.652920	0.77615	0.664865	0.89933	0.676811	0.05105

<u>Wavelength Response</u> <u>μm</u>		<u>Wavelength Response</u> <u>μm</u>		<u>Wavelength Response</u> <u>μm</u>		<u>Wavelength Response</u> <u>μm</u>	
0.677070	0.04749	0.681745	0.01520	0.686419	0.00571	0.691093	0.00213
0.677330	0.04407	0.682004	0.01437	0.686679	0.00562	0.691353	0.00203
0.677590	0.04082	0.682264	0.01351	0.686938	0.00528	0.691613	0.00187
0.677849	0.03812	0.682524	0.01276	0.687198	0.00489	0.691872	0.00169
0.678109	0.03537	0.682783	0.01213	0.687458	0.00473	0.692132	0.00161
0.678369	0.03297	0.683043	0.01148	0.687717	0.00454	0.692392	0.00149
0.678629	0.03084	0.683303	0.01091	0.687977	0.00427	0.692651	0.00134
0.678888	0.02910	0.683562	0.01034	0.688237	0.00407	0.692911	0.00127
0.679148	0.02732	0.683822	0.00995	0.688496	0.00391	0.693171	0.00115
0.679408	0.02570	0.684082	0.00941	0.688756	0.00355	0.693430	0.00102
0.679667	0.02426	0.684341	0.00884	0.689016	0.00341	0.693690	0.00093
0.679927	0.02295	0.684601	0.00841	0.689275	0.00326	0.693950	0.00082
0.680187	0.02156	0.684861	0.00798	0.689535	0.00312	0.694209	0.00085
0.680446	0.02024	0.685121	0.00750	0.689795	0.00274	0.694469	0.00082
0.680706	0.01914	0.685380	0.00709	0.690054	0.00259	0.694729	0.00062
0.680966	0.01806	0.685640	0.00685	0.690314	0.00240	0.694988	0.00060
0.681225	0.01695	0.685900	0.00653	0.690574	0.00232	0.695248	0.00057
0.681485	0.01589	0.686159	0.00616	0.690833	0.00224		

0.56µm

Wavelength µm	Response	Wavelength µm	Response	Wavelength µm	Response	Wavelength µm	Response
0.525153	0.00027	0.537159	0.00514	0.549165	0.52908	0.561171	0.86452
0.525414	0.00077	0.537420	0.00463	0.549426	0.58340	0.561432	0.84868
0.525675	0.00127	0.537681	0.00567	0.549687	0.63540	0.561693	0.83258
0.525936	0.00134	0.537942	0.00679	0.549948	0.68747	0.561954	0.81575
0.526197	0.00000	0.538203	0.00683	0.550209	0.73690	0.562215	0.80201
0.526458	0.00033	0.538464	0.00829	0.550470	0.78172	0.562476	0.78467
0.526719	0.00071	0.538725	0.00962	0.550731	0.81861	0.562737	0.77092
0.526980	0.00166	0.538986	0.00911	0.550992	0.85444	0.562998	0.75492
0.527241	0.00125	0.539247	0.00942	0.551253	0.88530	0.563259	0.74051
0.527502	0.00114	0.539508	0.01225	0.551514	0.91334	0.563520	0.72423
0.527763	0.00178	0.539769	0.01361	0.551775	0.93266	0.563781	0.71434
0.528024	0.00020	0.540030	0.01316	0.552036	0.94969	0.564042	0.69738
0.528285	0.00189	0.540291	0.01434	0.552297	0.96402	0.564303	0.68244
0.528546	0.00330	0.540552	0.01594	0.552558	0.97408	0.564564	0.66847
0.528807	0.00203	0.540813	0.01635	0.552819	0.98221	0.564825	0.65515
0.529068	0.00239	0.541074	0.01758	0.553080	0.98791	0.565086	0.64175
0.529329	0.00225	0.541335	0.02098	0.553341	0.99152	0.565347	0.62748
0.529590	0.00012	0.541596	0.02345	0.553602	0.99348	0.565608	0.61681
0.529851	0.00100	0.541857	0.02410	0.553863	0.99524	0.565869	0.60772
0.530112	0.00135	0.542118	0.02673	0.554124	0.99600	0.566130	0.59615
0.530373	0.00155	0.542379	0.03076	0.554385	0.99558	0.566391	0.58508
0.530634	0.00159	0.542640	0.03349	0.554646	0.99869	0.566652	0.57629
0.530895	0.00091	0.542901	0.03692	0.554907	1.00000	0.566913	0.56844
0.531156	0.00166	0.543162	0.04141	0.555168	0.99933	0.567174	0.56117
0.531417	0.00194	0.543423	0.04499	0.555429	0.99757	0.567435	0.55350
0.531678	0.00191	0.543684	0.04916	0.555690	0.99813	0.567696	0.54590
0.531939	0.00341	0.543945	0.05386	0.555951	0.99840	0.567957	0.54002
0.532200	0.00320	0.544206	0.06020	0.556212	0.99760	0.568218	0.53493
0.532461	0.00100	0.544467	0.06687	0.556473	0.99568	0.568479	0.53102
0.532722	0.00161	0.544728	0.07400	0.556734	0.99318	0.568740	0.52606
0.532983	0.00225	0.544989	0.08153	0.556995	0.99080	0.569001	0.52157
0.533244	0.00120	0.545250	0.08994	0.557256	0.98920	0.569262	0.51677
0.533505	0.00241	0.545511	0.10027	0.557517	0.98611	0.569523	0.51191
0.533766	0.00360	0.545772	0.11301	0.557778	0.98338	0.569784	0.50660
0.534027	0.00181	0.546033	0.12712	0.558039	0.97729	0.570045	0.50139
0.534288	0.00148	0.546294	0.14243	0.558300	0.97382	0.570306	0.49608
0.534549	0.00331	0.546555	0.16016	0.558561	0.96876	0.570567	0.48969
0.534810	0.00371	0.546816	0.18023	0.558822	0.96119	0.570828	0.48316
0.535071	0.00373	0.547077	0.20268	0.559083	0.95394	0.571089	0.47587
0.535332	0.00477	0.547338	0.23190	0.559344	0.94531	0.571350	0.46756
0.535593	0.00458	0.547599	0.26305	0.559605	0.93768	0.571611	0.45783
0.535854	0.00438	0.547860	0.29721	0.559866	0.92832	0.571872	0.44391
0.536115	0.00439	0.548121	0.33444	0.560127	0.91625	0.572133	0.43223
0.536376	0.00494	0.548382	0.37909	0.560388	0.90409	0.572394	0.41863
0.536637	0.00521	0.548643	0.42754	0.560649	0.89134	0.572655	0.40284
0.536898	0.00599	0.548904	0.47697	0.560910	0.87716	0.572916	0.38479

<u>Wavelength μm</u>	<u>Response</u>	<u>Wavelength μm</u>	<u>Response</u>	<u>Wavelength μm</u>	<u>Response</u>	<u>Wavelength μm</u>	<u>Response</u>
0.573177	0.36790	0.577875	0.09572	0.582573	0.02702	0.587271	0.00970
0.573438	0.35028	0.578136	0.08770	0.582834	0.02556	0.587532	0.00970
0.573699	0.32990	0.578397	0.08146	0.583095	0.02468	0.587793	0.00892
0.573960	0.30917	0.578658	0.07565	0.583356	0.02279	0.588054	0.00800
0.574221	0.29001	0.578919	0.07040	0.583617	0.02058	0.588315	0.00836
0.574482	0.26999	0.579180	0.06567	0.583878	0.01963	0.588576	0.00807
0.574743	0.25048	0.579441	0.06198	0.584139	0.01894	0.588837	0.00669
0.575004	0.23221	0.579702	0.05732	0.584400	0.01742	0.589098	0.00644
0.575265	0.21434	0.579963	0.05321	0.584661	0.01677	0.589359	0.00708
0.575526	0.19870	0.580224	0.04966	0.584922	0.01549	0.589620	0.00680
0.575787	0.18446	0.580485	0.04624	0.585183	0.01476	0.589881	0.00567
0.576048	0.17049	0.580746	0.04223	0.585444	0.01495	0.590142	0.00507
0.576309	0.15626	0.581007	0.03974	0.585705	0.01498	0.590403	0.00496
0.576570	0.14414	0.581268	0.03741	0.585966	0.01324	0.590664	0.00500
0.576831	0.13386	0.581529	0.03439	0.586227	0.01207	0.590925	0.00508
0.577092	0.12275	0.581790	0.03231	0.586488	0.01240	0.591186	0.00476
0.577353	0.11217	0.582051	0.03115	0.586749	0.01217	0.591447	0.00404
0.577614	0.10372	0.582312	0.02940	0.587010	0.01039		

Appendix D Source Calibration - Raw Data

Aperture No.	Diameter (mm)	Radiometer Reading (nW)				
		1.6µm Northern Optics	0.87µm ATSR-2	AATSR	0.66µm AATSR	0.56µm AATSR
390 W Lamp Setting						
27	200.0	13780	55030	41960	28430	11500
26	150.0	13722	32730	24900	17020	6871
25	130.0	10260	24600	18710	12820	5117
24	100.5	6143	14860	11310	7772	3135
23	79.8	3903	9459	7194	4954	1998
22	70.0	3019	7323	5572	3841	1550
21	63.1	2432	5905	4490	3097	1249
20	50.4	1552	3775	2870	1981	799
19	42.6	1118	2715	2067	1425	576
18	35.2	763	1853	1412	974	392
17	30.6	577	1402	1067	735	297
16	25.6	402	975	742	512	207
15	22.0	297	721	550	379	153
14	17.4	190	459	350	242	98
13	15.0	140	337	256	177	71
12	12.4	97	232	178	122	49
11	11.1	77	186	142	98	40
10	8.8	47	113	86	59	24
9	7.6	36	86	65	45	18
8	6.0	23	53	40	28	11
7	5.4	19	44	33	23	9
6	4.4		29	22	15	6
5	3.8		21	16	11	5
4	2.9		13	10	7	3
3	2.5		9	7	5	2
2	2.0		6	4	3	1
1	1.0		1	1	1	0
0	0.0	1	0	0	0	0
240W Lamp Setting						
27	200.0	14380	32980	25000	17050	6914
26	150.0		19640	14920	10230	4135
25	130.0		14760	11230	7695	3114
24	100.5		8903	6793	4660	1889
23	79.8		5665	4323	2971	1204
22	70.0		4387	3345	2304	938
21	63.1		3538	2698	1857	752
20	50.4		2258	1725	1187	482
19	42.6		1628	1241	854	346
18	35.2		1110	847	584	237
17	30.6		839	641	441	179
16	25.6	243	584	445	307	125

Aperture No.	Diameter (mm)	Radiometer Reading (nW)				
		1.6μm Northern Optics	0.87μm ATSR-2	AATSR	0.66μm AATSR	0.56μm AATSR
15	22.0		433	330	227	92
14	17.4		275	209	145	59
13	15.0		202	154	106	43
12	12.4		139	106	73	30
11	11.1		112	85	59	24
10	8.8		68	52	36	14
9	7.6		51	39	27	11
8	6.0		32	24	17	7
7	5.4		26	20	14	6
6	4.4		17	13	9	4
5	3.8		13	10	7	3
4	2.9		8	6	4	2
3	2.5		5	4	3	1
2	2.0		3	3	2	1
1	1.0		1	1	0	0
0	0.0		0	0	0	0
150 W Lamp Setting						
27	200.0	9668	22260	16840	11480	4633
26	150.0		13260	10062	6871	2774
25	130.0		9989	7564	5172	2087
24	100.5		6010	4571	3136	1265
23	79.8		3830	2910	2000	806
22	70.0		2929	2254	1551	625
21	63.1		2392	1817	1251	504
20	50.4		1529	1161	799	322
19	42.6		1099	835	575	232
18	35.2		751	571	393	158
17	30.6		567	431	297	120
16	25.6	164	395	300	207	83
15	22.0		292	223	153	62
14	17.4		186	142	97	39
13	15.0		136	104	71	29
12	12.4		94	72	49	20
11	11.1		75	57	39	16
10	8.8		46	35	24	10
9	7.6		35	26	18	7
8	6.0		21	16	11	5
7	5.4		18	14	9	4
6	4.4		12	9	6	2
5	3.8		9	7	5	2
4	2.9		5	4	3	1
3	2.5		4	3	2	1
2	2.0		2	2	1	0
1	1.0		1	0	0	0
0	0.0		0	0	0	0

Aperture No.	Diameter (mm)	Radiometer Reading (nW)				
		1.6 μ m Northern Optics	0.87 μ m ATSR-2	AATSR	0.66 μ m AATSR	0.56 μ m AATSR
45W Lamp Setting						
27	200.0	4674	10864	8212	5707	2320
26	150.0		6463	4895	3402	1388
25	130.0		4835	3685	2556	1047
24	100.5		2928	2228	1553	635
23	79.8		1865	1418	990	406
22	70.0		1444	1098	768	314
21	63.1		1163	886	618	253
20	50.4		743	566	395	162
19	42.6		534	407	285	117
18	35.2		365	279	194	80
17	30.6		276	210	147	60
16	25.6	79	192	146	102	42
15	22.0		142	108	76	31
14	17.4		91	69	48	20
13	15.0		66	50	35	14
12	12.4		46	35	24	10
11	11.1		37	28	20	8
10	8.8		22	17	12	5
9	7.6		17	13	9	4
8	6.0		10	8	6	2
7	5.4		9	7	5	2
6	4.4		6	4	3	1
5	3.8		4	3	2	1
4	2.9		3	2	1	1
3	2.5		2	1	1	0
2	2.0		1	1	1	0
1	1.0		0	0	0	0
0	0.0		0	0	0	0
45W Lamp Setting						
27	200.0	2334	5450	4116	2845	1167
26	150.0		3239	2458	1704	698
25	130.0		2438	1849	1286	527
24	100.5		1473	1118	780	318
23	79.8		938	713	497	203
22	70.0		726	550	386	157
21	63.1		585	444	311	127
20	50.4		374	284	199	81
19	42.6		269	204	143	58
18	35.2		184	139	98	40
17	30.6		139	105	74	30
16	25.6	40	97	73	51	21
15	22.0		72	54	38	16
14	17.4		46	35	24	10
13	15.0		33	25	18	7
12	12.4		23	17	12	5

Aperture No.	Diameter (mm)	Radiometer Reading (nW)				
		1.6 μ m Northern Optics	0.87 μ m ATSR-2	AATSR	0.66 μ m AATSR	0.56 μ m AATSR
11	11.1		18	14	10	4
10	8.8		11	9	6	2
9	7.6		9	6	5	2
8	6.0		5	4	3	1
7	5.4		4	3	2	1
6	4.4		3	2	2	1
5	3.8		2	2	1	0
4	2.9		1	1	1	0
3	2.5		1	1	0	0
2	2.0		1	0	0	0
1	1.0		0	0	0	0
0	0.0		0	0	0	0

Appendix E Calibrated AATSR Input Radiances

Aperture	Radiance mWcm ⁻² sr ⁻¹			
	1.6μm	0.87μm	0.66μm	0.56μm
390 W Lamp Setting				
27	2.2824E+00	2.2396E+00	1.7331E+00	1.0359E+00
26	2.3183E+00	2.3738E+00	1.8438E+00	1.1016E+00
25	2.3298E+00	2.3771E+00	1.8481E+00	1.1028E+00
24	1.9571E+00	2.0080E+00	1.5657E+00	9.3519E-01
23	1.2380E+00	1.2783E+00	9.9830E-01	5.9638E-01
22	9.5243E-01	9.8923E-01	7.7416E-01	4.6271E-01
21	7.7540E-01	7.9757E-01	6.2410E-01	3.7249E-01
20	4.9624E-01	5.0976E-01	3.9890E-01	2.3839E-01
19	3.5370E-01	3.6682E-01	2.8714E-01	1.7140E-01
18	2.4126E-01	2.5057E-01	1.9606E-01	1.1707E-01
17	1.8241E-01	1.8927E-01	1.4818E-01	8.8533E-02
16	1.2774E-01	1.3171E-01	1.0315E-01	6.1667E-02
15	9.4487E-02	9.7642E-02	7.6328E-02	4.5638E-02
14	5.9441E-02	6.1996E-02	4.8624E-02	2.9049E-02
13	4.3682E-02	4.5472E-02	3.5607E-02	2.1279E-02
12	3.0053E-02	3.1413E-02	2.4569E-02	1.4691E-02
11	2.4213E-02	2.5193E-02	1.9700E-02	1.1784E-02
10	1.4966E-02	1.5270E-02	1.1941E-02	7.1451E-03
9	1.1320E-02	1.1608E-02	9.0714E-03	5.4300E-03
8	6.9436E-03	7.1589E-03	5.5987E-03	3.3461E-03
7	5.7212E-03	5.9186E-03	4.6383E-03	2.7807E-03
6	3.7673E-03	3.8654E-03	3.0267E-03	1.8057E-03
5	2.7489E-03	2.8956E-03	2.2694E-03	1.3558E-03
4	1.6782E-03	1.7644E-03	1.3809E-03	8.2529E-04
3	1.1830E-03	1.2290E-03	9.6164E-04	5.7667E-04
2	7.4332E-04	7.7008E-04	5.9964E-04	3.6018E-04
1	1.7642E-04	1.8256E-04	1.4579E-04	8.5131E-05
0	0.0000E+00	0.0000E+00	0.0000E+00	0.0000E+00
240W Lamp Setting				
27	1.3644E+00	1.3402E+00	1.0326E+00	6.2077E-01
26	1.3859E+00	1.4205E+00	1.0986E+00	6.6014E-01
25	1.3928E+00	1.4225E+00	1.1011E+00	6.6087E-01
24	1.1700E+00	1.2017E+00	9.3286E-01	5.6043E-01
23	7.4004E-01	7.6495E-01	5.9479E-01	3.5740E-01
22	5.6936E-01	5.9199E-01	4.6125E-01	2.7729E-01
21	4.6353E-01	4.7729E-01	3.7184E-01	2.2322E-01
20	2.9665E-01	3.0506E-01	2.3766E-01	1.4286E-01
19	2.1144E-01	2.1952E-01	1.7108E-01	1.0271E-01
18	1.4423E-01	1.4995E-01	1.1681E-01	7.0154E-02

Aperture	Radiance mWcm ⁻² sr ⁻¹			
	1.6μm	0.87μm	0.66μm	0.56μm
17	1.0905E-01	1.1326E-01	8.8286E-02	5.3055E-02
16	7.6361E-02	7.8822E-02	6.1457E-02	3.6955E-02
15	5.6484E-02	5.8432E-02	4.5476E-02	2.7350E-02
14	3.5533E-02	3.7100E-02	2.8971E-02	1.7408E-02
13	2.6113E-02	2.7212E-02	2.1215E-02	1.2752E-02
12	1.7966E-02	1.8799E-02	1.4638E-02	8.8036E-03
11	1.4474E-02	1.5076E-02	1.1737E-02	7.0620E-03
10	8.9463E-03	9.1377E-03	7.1146E-03	4.2818E-03
9	6.7672E-03	6.9466E-03	5.4047E-03	3.2541E-03
8	4.1509E-03	4.2841E-03	3.3357E-03	2.0052E-03
7	3.4201E-03	3.5418E-03	2.7635E-03	1.6664E-03
6	2.2521E-03	2.3132E-03	1.8033E-03	1.0821E-03
5	1.6433E-03	1.7328E-03	1.3521E-03	8.1249E-04
4	1.0032E-03	1.0559E-03	8.2274E-04	4.9457E-04
3	7.0717E-04	7.3545E-04	5.7295E-04	3.4558E-04
2	4.4435E-04	4.6084E-04	3.5727E-04	2.1585E-04
1	1.0546E-04	1.0925E-04	8.6864E-05	5.1017E-05
0	0.0000E+00	0.0000E+00	0.0000E+00	0.0000E+00
150W Lamp Setting				
27	9.3435E-01	9.1897E-01	7.0749E-01	4.2235E-01
26	9.4905E-01	9.7402E-01	7.5271E-01	4.4913E-01
25	9.5375E-01	9.7540E-01	7.5443E-01	4.4963E-01
24	8.0117E-01	8.2395E-01	6.3917E-01	3.8130E-01
23	5.0678E-01	5.2451E-01	4.0753E-01	2.4316E-01
22	3.8989E-01	4.0591E-01	3.1603E-01	1.8866E-01
21	3.1742E-01	3.2727E-01	2.5477E-01	1.5187E-01
20	2.0315E-01	2.0917E-01	1.6284E-01	9.7198E-02
19	1.4479E-01	1.5052E-01	1.1722E-01	6.9884E-02
18	9.8765E-02	1.0281E-01	8.0036E-02	4.7731E-02
17	7.4674E-02	7.7662E-02	6.0491E-02	3.6097E-02
16	5.2292E-02	5.4046E-02	4.2109E-02	2.5143E-02
15	3.8680E-02	4.0065E-02	3.1159E-02	1.8608E-02
14	2.4333E-02	2.5439E-02	1.9850E-02	1.1844E-02
13	1.7882E-02	1.8658E-02	1.4536E-02	8.6759E-03
12	1.2303E-02	1.2890E-02	1.0030E-02	5.9897E-03
11	9.9120E-03	1.0338E-02	8.0422E-03	4.8047E-03
10	6.1264E-03	6.2655E-03	4.8747E-03	2.9132E-03
9	4.6341E-03	4.7631E-03	3.7032E-03	2.2140E-03
8	2.8425E-03	2.9375E-03	2.2855E-03	1.3643E-03
7	2.3421E-03	2.4286E-03	1.8935E-03	1.1338E-03
6	1.5422E-03	1.5861E-03	1.2356E-03	7.3624E-04
5	1.1253E-03	1.1882E-03	9.2644E-04	5.5279E-04
4	6.8699E-04	7.2399E-04	5.6372E-04	3.3649E-04
3	4.8427E-04	5.0428E-04	3.9257E-04	2.3512E-04

Aperture	Radiance mWcm ⁻² sr ⁻¹			
	1.6μm	0.87μm	0.66μm	0.56μm
2	3.0429E-04	3.1599E-04	2.4479E-04	1.4685E-04
1	7.2221E-05	7.4911E-05	5.9517E-05	3.4710E-05
0	0.0000E+00	0.0000E+00	0.0000E+00	0.0000E+00
90W Lamp Setting				
27	4.5523E-01	4.4834E-01	3.4442E-01	2.0670E-01
26	4.6239E-01	4.7520E-01	3.6643E-01	2.1981E-01
25	4.6468E-01	4.7587E-01	3.6728E-01	2.2005E-01
24	3.9034E-01	4.0198E-01	3.1116E-01	1.8661E-01
23	2.4691E-01	2.5589E-01	1.9840E-01	1.1900E-01
22	1.8996E-01	1.9803E-01	1.5385E-01	9.2330E-02
21	1.5465E-01	1.5966E-01	1.2403E-01	7.4327E-02
20	9.8975E-02	1.0205E-01	7.9275E-02	4.7569E-02
19	7.0544E-02	7.3433E-02	5.7065E-02	3.4201E-02
18	4.8120E-02	5.0161E-02	3.8963E-02	2.3360E-02
17	3.6382E-02	3.7889E-02	2.9448E-02	1.7666E-02
16	2.5477E-02	2.6368E-02	2.0499E-02	1.2305E-02
15	1.8845E-02	1.9547E-02	1.5169E-02	9.1068E-03
14	1.1855E-02	1.2411E-02	9.6633E-03	5.7966E-03
13	8.7124E-03	9.1030E-03	7.0763E-03	4.2461E-03
12	5.9941E-03	6.2886E-03	4.8827E-03	2.9314E-03
11	4.8293E-03	5.0434E-03	3.9151E-03	2.3515E-03
10	2.9849E-03	3.0568E-03	2.3731E-03	1.4258E-03
9	2.2578E-03	2.3238E-03	1.8028E-03	1.0835E-03
8	1.3849E-03	1.4331E-03	1.1127E-03	6.6769E-04
7	1.1411E-03	1.1848E-03	9.2178E-04	5.5487E-04
6	7.5138E-04	7.7382E-04	6.0151E-04	3.6032E-04
5	5.4827E-04	5.7967E-04	4.5101E-04	2.7054E-04
4	3.3471E-04	3.5322E-04	2.7443E-04	1.6468E-04
3	2.3594E-04	2.4603E-04	1.9111E-04	1.1507E-04
2	1.4825E-04	1.5416E-04	1.1917E-04	7.1871E-05
1	3.5187E-05	3.6547E-05	2.8974E-05	1.6987E-05
0	0.0000E+00	0.0000E+00	0.0000E+00	0.0000E+00
45W Lamp Setting				
27	2.3139E-01	2.2702E-01	1.7503E-01	1.0476E-01
26	2.3503E-01	2.4063E-01	1.8622E-01	1.1140E-01
25	2.3619E-01	2.4097E-01	1.8664E-01	1.1153E-01
24	1.9841E-01	2.0355E-01	1.5813E-01	9.4579E-02
23	1.2550E-01	1.2958E-01	1.0082E-01	6.0315E-02
22	9.6555E-02	1.0028E-01	7.8185E-02	4.6795E-02
21	7.8608E-02	8.0848E-02	6.3030E-02	3.7671E-02
20	5.0308E-02	5.1674E-02	4.0286E-02	2.4109E-02
19	3.5857E-02	3.7184E-02	2.8999E-02	1.7334E-02
18	2.4459E-02	2.5400E-02	1.9801E-02	1.1839E-02
17	1.8493E-02	1.9186E-02	1.4965E-02	8.9537E-03

Aperture	Radiance mWcm ⁻² sr ⁻¹			
	1.6μm	0.87μm	0.66μm	0.56μm
16	1.2950E-02	1.3352E-02	1.0417E-02	6.2366E-03
15	9.5789E-03	9.8978E-03	7.7086E-03	4.6156E-03
14	6.0259E-03	6.2844E-03	4.9108E-03	2.9379E-03
13	4.4284E-03	4.6094E-03	3.5961E-03	2.1520E-03
12	3.0467E-03	3.1843E-03	2.4813E-03	1.4857E-03
11	2.4547E-03	2.5538E-03	1.9896E-03	1.1918E-03
10	1.5172E-03	1.5478E-03	1.2060E-03	7.2261E-04
9	1.1476E-03	1.1767E-03	9.1615E-04	5.4916E-04
8	7.0392E-04	7.2568E-04	5.6543E-04	3.3840E-04
7	5.8000E-04	5.9995E-04	4.6843E-04	2.8122E-04
6	3.8192E-04	3.9183E-04	3.0568E-04	1.8262E-04
5	2.7868E-04	2.9352E-04	2.2920E-04	1.3712E-04
4	1.7013E-04	1.7886E-04	1.3946E-04	8.3465E-05
3	1.1993E-04	1.2458E-04	9.7120E-05	5.8321E-05
2	7.5355E-05	7.8062E-05	6.0560E-05	3.6426E-05
1	1.7885E-05	1.8506E-05	1.4724E-05	8.6096E-06
0	0.0000E+00	0.0000E+00	0.0000E+00	0.0000E+00

Appendix F Test Data Files

Test	Description	Condition	Level1 File	Raw Data File
VIS01	Calibration of Integrating Sphere			ISPHERE.LUT
VIS02	Visible Channel Responsivity	Ambient	VIS02\$05-NOV-1997.LEV1	VIS02\$05-NOV-1997.PKT
			VIS02\$05-NOV-1997.LEV1	VIS02\$05-NOV-1997.PKT
		FPA in Vacuum	VIS02\$28-OCT-1997.LEV1	VIS02\$28-OCT-1997.PKT
			VIS02\$29-OCT-1997.LEV1	VIS02\$29-OCT-1997.PKT
		IRFPA at 80K	VIS02\$31-OCT-1997.LEV1	VIS02\$31-OCT-1997.PKT
VIS03	Visible Calibration with different Gain	Ambient	VIS03\$06-NOV-1997.LEV1	VIS03\$06-NOV-1997.PKT
		IRFPA at 80K	VIS03\$31-OCT-1997.LEV1	VIS03\$31-OCT-1997.PKT
			VIS03\$02-NOV-1997.LEV1	VIS03\$02-NOV-1997.PKT
VIS04	Visible Calibration around Scan	Ambient	VIS04\$06-NOV-1997.LEV1	VIS04\$06-NOV-1997.PKT
VIS05	Calibration of VISCAL unit	Ambient	VIS05\$05-NOV-1997.LEV1	VIS05\$05-NOV-1997.PKT
		FPA in Vacuum	VIS05\$29-OCT-1997.LEV1	VIS05\$29-OCT-1997.PKT
		IRFPA at 80K	VIS05\$30-OCT-1997.LEV1	VIS05\$30-OCT-1997.PKT
VIS06	VISCAL Field of View	IRFPA at 80K	VIS06\$04-NOV-1997.PIX	VIS06\$04-NOV-1997.PKT
VIS07	Visible Channel Polarisation	Ambient	VIS07\$06-NOV-1997.LEV1	VIS07\$06-NOV-1997.PKT
		IRFPA at 80K	VIS07\$02-NOV-1997.LEV1	VIS07\$02-NOV-1997.PKT
VIS08*	Transmission of ZnS Window	Ambient	VIS08\$06-NOV-1997.LEV1	VIS08\$06-NOV-1997.PKT
VIS08	Repeat Visible Channel Responsivity	Ambient	VIS08\$12-OCT-1998.LEV1	VIS08\$12-OCT-1998.PKT
		FPA in Vacuum	VIS08\$07-OCT-1998.LEV1	VIS08\$07-OCT-1998.PKT
		IR FPA at 80K	VIS08\$09-OCT-1998.LEV1	VIS08\$09-OCT-1998.PKT
VIS09	Repeat VISCAL Throughput	Ambient	VIS09\$12-OCT-1998.LEV1	VIS09\$12-OCT-1998.PKT
		FPA in Vacuum	VIS09\$08-OCT-1998.LEV1	VIS09\$08-OCT-1998.PKT
		IR FPA at 80K	VIS09\$08-OCT-1998.LEV1	VIS09\$08-OCT-1998.PKT
			VIS09\$09-OCT-1998.LEV1	VIS09\$09-OCT-1998.PKT
VIS10	Transmission of ZnSe Window	Ambient	VIS10\$12-OCT-1998.LEV1	VIS10\$12-OCT-1998.PKT